Published in final edited form as:
Nat Cardiovasc Res. 2022 November ; 1: 1056–1071. doi:10.1038/s44161-022-00155-0.

GPR55 in B cells limits atherosclerosis development and regulates plasma cell maturation

Raquel Guillamat-Prats[1], **Daniel Hering**[1], **Abhishek Derle**[1], **Martina Rami**[1], **Carmen Härdtner**[3], **Donato Santovito**[1,2,5], **Petteri Rinne**[6], **Laura Bindila**[7], **Michael Hristov**[1], **Sabrina Pagano**[8], **Nicolas Vuilleumier**[8], **Sofie Schmid**[9], **Aleksandar Janjic**[10], **Wolfgang Enard**[10], **Christian Weber**[1,2,11,12], **Lars Maegdefessel**[2,9], **Alexander Faussner**[1], **Ingo Hilgendorf**[3,4], **Sabine Steffens**[1,2,*]

[1]Institute for Cardiovascular Prevention (IPEK), Ludwig-Maximilians-Universität (LMU) Munich, Munich, Germany

[2]German Center for Cardiovascular Research (DZHK), Partner Site Munich Heart Alliance (MHA), Munich, Germany

[3]Department of Cardiology and Angiology I, Heart Center and Faculty of Medicine, University of Freiburg. Freiburg, Germany

[4]Institute for Experimental Cardiovascular Medicine, Heart Center and Faculty of Medicine, University of Freiburg, Freiburg, Germany

[5]Institute for Genetic and Biomedical Research (IRGB), Unit of Milan, National Research Council, Milan, Italy

[6]Institute of Biomedicine, University of Turku, Turku, Finland

[7]Institute of Physiological Chemistry, University Medical Center of the Johannes Gutenberg University Mainz, Mainz, Germany

[8]Division of Laboratory Medicine, Diagnostic Department, Geneva University Hospitals and Faculty of Medicine

[9]Department of Vascular and Endovascular Surgery, Klinikum rechts der Isar - Technical University Munich (TUM), Munich, Germany

*Correspondence: Sabine Steffens, Institute for Cardiovascular Prevention (IPEK), Ludwig-Maximilians-Universität (LMU) Munich, Munich, Germany; sabine.steffens@med.uni-muenchen.de.

Author contributions

R.G.-P., D.H. and M.R. designed and performed experiments and analyzed and interpreted data supervised by S.S.. A.D. contributed to the *in vivo* revision experiments and tested GPR55 antibody specificity by Western blotting. C.H. and I.H. designed the B-cell bone marrow transplant experiment, and I.H. gave critical input for the entire study design. D.S. provided expertise for confocal/STED imaging and statistical analysis. P.R. contributed to the histological analysis. L.B. performed lipidomic measurements. S.P. and N.V. determined MDA-oxLDL antibodies in plasma. M.H. conducted cell sorting. A.J. and W.E. performed the bulk RNA-sequencing and the clean-up of the obtained data. S.Sch. and L.M. determined *GPR55* expression in human plaques. A.F. guided the Ca^{2+} assays and provided critical input to the study. C.W. provided scientific infrastructure and advice for the study design. R.G.-P. and S.S. designed the study and wrote the manuscript. All authors contributed to the final manuscript editing and approved the submitted version.

Competing interests

The authors declare no conflicts of interests.

Europe PMC Funders Author Manuscripts

[10]Anthropology and Human Genomics, Faculty of Biology, Ludwig-Maximilians University, Martinsried, Germany

[11]Department of Biochemistry, Cardiovascular Research Institute Maastricht (CARIM), Maastricht University Medical Centre, 6229 ER Maastricht, The Netherlands

[12]Munich Cluster for Systems Neurology (SyNergy), Munich, Germany

Abstract

Dissecting the pathways regulating the adaptive immune response in atherosclerosis is of particular therapeutic interest. Here we report that the lipid G-protein coupled receptor GPR55 is highly expressed by splenic plasma cells (PC), upregulated in mouse spleens during atherogenesis and human unstable or ruptured compared to stable plaques. *Gpr55*-deficient mice developed larger atherosclerotic plaques with increased necrotic core size compared to their corresponding controls. Lack of GPR55 hyperactivated B cells, disturbed PC maturation and resulted in immunoglobulin (Ig)G overproduction. B cell-specific *Gpr55* depletion or adoptive transfer of *Gpr55*-deficient B cells was sufficient to promote plaque development and elevated IgG titers. *In vitro*, the endogenous GPR55 ligand lysophsophatidylinositol (LPI) enhanced PC proliferation, whereas GPR55 antagonism blocked PC maturation and increased their mitochondrial content. Collectively, these discoveries provide previously undefined evidence for GPR55 in B cells as a key modulator of the adaptive immune response in atherosclerosis.

Introduction

Cardiovascular diseases (CVDs) related to atherosclerosis are the leading cause of death worldwide. Atherosclerosis is a chronic and multifactorial disease involving both arms of our immune system, the innate and adaptive immunity.[1–3] Recent advances in analytical approaches such as single cell sequencing and mass cytometry have deepened our knowledge about the cellular heterogeneity within the atherosclerotic lesions,[4] supporting the relevance of B lymphocytes in the pathophysiology of the disease.

Diverse subset-specific functions of B cells in atherosclerosis have been described over the last years, reporting both pro- and antiatherogenic properties.[5–8] For example, B1a cells are considered as main producers of naturally occurring IgM antibodies arising without antigen-mediated induction. These antibodies recognize oxidation-specific epitopes (OSE) that are present on lipoprotein particles as well as apoptotic cells, thereby limiting atherosclerotic plaque progression.[8] The B2 lineage can be separated into marginal zone (MZ) and follicular (FO) cells. While MZ cells are positioned at the splenic red pulp border to scan the blood for circulating antigens, FO cells interact with T follicular helper (Tfh) cells to initiate the germinal center (GC) response.[9] This culminates in the final stage of B cell maturation, which involves the rapid proliferation of plasmablasts secreting low antibody levels, somatic hypermutations in the B cell receptor (BCR) region and selection of high antigen affinity clones to ultimately differentiate into long-lived PCs.[10] PCs have a high protein synthesis capacity and secrete large amounts of antibodies into the circulation, which depends on a set of transcription factors, including PR domain zinc finger protein 1 (BLIMP1), interferon regulatory factor 4 (IRF4) and X-box binding protein 1 (XBP1). Antigen-specific antibodies

of various isotypes, including IgGs, are produced by class-switching of the high affinity B cell clones.

In the context of atherosclerosis, IgGs have been reported to form immune complexes with oxLDL and promote macrophage inflammatory responses.[11] High-throughput single-cell analysis of the atherosclerosis-associated antibody repertoire recently discovered atheroprotective anti-ALDH4A1 autoantibodies directed against a mitochondrial dehydrogenase.[12] MZ B cells have been shown to negatively control pro-atherogenic Tfh responses to hypercholesterolemia,[13] which underlines the complexity of B cell subset-specific functions and autoantibodies in atherosclerosis.

B cell activation involves antigen binding to the BCRs, which are membrane-bound immunoglobulins with unique epitope-binding sites expressed by each clone. The BCRs form a signaling complex with other receptors on the B cell surface, including among other, receptor-type tyrosine-protein phosphatase C (PTPRC, also known as B220).[11]

GPR55 is a G protein-coupled orphan receptor expressed by various leukocyte subsets, including B and T cells, but also natural killer cells, monocytes, macrophages, and neutrophils. According to murine immune cell transcriptomic data (Immgen.org),[14] GPR55 is highly expressed by splenic PCs and, to a lower extent, MZ B cells. The most potent endogenous GPR55 ligand identified so far is lysophosphatidylinositol (LPI), [15–17] which is synthesized by the enzyme phospholipase DDHD domain containing 1 (DDHD1). Within the spleen, this enzyme is mostly expressed by conventional CD4+ and CD8+ dendritic cells as well as red pulp macrophages (Immgen.org).[14] Immunological functions for GPR55 have been described, amongst others, in γδT cells residing in intestinal lymphoid organs, where *Gpr55* deficiency or short-term antagonist treatment protected mice from nonsteroidal anti-inflammatory drug-induced increases in intestinal permeability.[18]

In THP1-derived macrophages, GPR55 stimulation promoted the accumulation of oxidized LDL and blocked cholesterol efflux, while GPR55 antagonism counteracted these effects.[19] In aortic endothelial cells, antagonizing GPR55 with CID16020046 prevented ox-LDL-induced inflammatory stress.[20] *In vivo* treatment of atherosclerosis-prone *Apoe*$^{-/-}$ mice with CID16020046 reduced neutrophil recruitment and plaque infiltration, while no effects on plaque size were detectable.[21] However, the role of GPR55 in regulating adaptive B cell responses in the context of atherosclerosis has not been investigated so far.

Using a global *Gpr55* knockout mouse model, B cell specific deletion and adoptive transfer experiments, we report here that GPR55 plays a pleiotropic role in the B cell compartment, which crucially affects atherosclerosis. Our findings provide further insight into the complex regulation of humoral immunity and might be of broader relevance beyond atherosclerosis, such as autoimmune disorders.

Results

Modulation and role of the GPR55-LPI axis in atherosclerosis

To address the regulation of the GPR55-LPI axis during hypercholesterolemia, we fed apolipoprotein E-deficient (*Apoe*$^{-/-}$) mice with Western diet (WD) for 4 or 16 weeks, respectively, and measured LPI plasma levels by liquid chromatography-tandem mass spectrometry. Circulating LPI was elevated during the early stage of atherogenesis and returned to baseline concentrations after 16 weeks WD (Fig. 1A). Given that GPR55 is highly expressed by splenic B cells, we focused on the spleen to assess a modulation of the receptor and the LPI synthesizing enzyme DDHD1 during atherosclerosis onset and progression. In accordance with the modulation of plasma LPI levels, *Ddhd1* was upregulated after 4, but not 16 weeks WD (Fig. 1B). A similar pattern for the splenic *Gpr55* mRNA expression was observed (Fig. 1C). At the 4-week time point, the splenic GPR55 expression inversely correlated with aortic root atherosclerotic plaque size (Fig. 1D), suggesting that GPR55 signaling may exert an early protective effect on plaque development. The causal implication of GPR55 in atherogenesis was substantiated in *Apoe*$^{-/-}$ *Gpr55*$^{-/-}$ mice receiving 4 weeks WD, which developed larger plaques within aortic roots compared to corresponding *Apoe*$^{-/-}$ controls (Fig. 1E-G). These findings suggest that GPR55 signaling counterbalances plaque development, at least in early disease stage. To address the question if *Gpr55* deficiency may affect LPI levels, we compared splenic transcript levels of the LPI-producing enzyme *Ddhd1* between *Apoe*$^{-/-}$ and *Apoe-/-Gpr55*$^{-/-}$ mice and detected higher levels in *Gpr55*-deficient mice. Nevertheless, the relative expression levels followed a similar pattern over the course of atherogenic diet feeding as observed in *Apoe*$^{-/-}$ mice (Fig. 1H). After 10 weeks of WD, the plaque burden was higher in the descending aorta in *Apoe*$^{-/-}$*Gpr55*$^{-/-}$ mice compared to *Apoe*$^{-/-}$ mice (Extended Data Fig. 1A). After 16 weeks WD, a more in-depth characterization of the plaque development revealed that the difference in aortic lesion area was no longer observed at this advanced stage (Extended Data Fig. 1B). In the descending aorta, however, the plaque burden was still higher in *Apoe*$^{-/-}$*Gpr55*$^{-/-}$ mice (Extended Data Fig. 1C). This might reflect stage dependent effects of GPR55 during atherosclerosis, since plaque development in descending aortas is generally less advanced compared to aortic root plaques in mouse models of atherosclerosis.[22] In support of this hypothesis, 16-weeks-plaques of *Gpr55*-deficient mice exhibited an increased necrotic core and collagen area, but decreased relative plaque content of macrophages and lipids, indicative of a more advanced plaque phenotype (Extended Data Fig. 1D to G). These effects of *Gpr55* deficiency on the advanced plaque phenotype support a possible relevance for complications in human atherosclerosis pathophysiology.

To validate the expression and possible modulation of GPR55 in human plaques, we analyzed the transcript levels in stable and unstable carotid artery plaques collected from patients undergoing endarterectomy. The plaque phenotype was assigned based on the morphology following the American Heart Association (AHA) classification[23] with or without a vulnerable fibrous cap according to Redgrave et al.[24] (Fig. 1I and Extended Data Table 4, patient characteristics). The qPCR analysis revealed reduced *GPR55* expression in unstable compared to stable plaques (Fig. 1J), which might suggest that high expression

Europe PMC Funders Author Manuscripts

levels of this receptor may counterbalance the patient's risk for developing an acute cardiovascular event.

B cell *Gpr55* expression and functionality

We next assessed the expression profile of *Gpr55* in sorted murine blood leukocytes of *Apoe*$^{-/-}$ mice by digital droplet PCR (ddPCR) and qPCR. The rank order of *Gpr55* expression in the different populations was B cells > T cells > neutrophils > monocytes, which was consistently confirmed by both techniques (Fig. 2A). Moreover, we determined *Gpr55* expression in different B cell subsets, which confirmed a higher expression in PCs compared to GC B cells, followed by B2 and B1 subsets (Fig. 2A). By *in situ* hybridization, we localized *Gpr55* expression in the splenic B cell FO and GC areas (Fig. 2B).

The functional GPR55 signaling response in B cells was subsequently validated by measuring intracellular calcium (Ca^{2+}) increases in response to stimulation with the endogenous GPR55 ligand LPI. We tested a soybean extract with a mix of different LPI species and pure 20:4-LPI, the specific ligand for GPR55, in circulating B cells of *Apoe*$^{-/-}$ mice, both in normal diet condition and hypercholesterolemia after 10 weeks WD, as well as circulating B cells of WT mice under normal diet condition. Independent of the genetic background or diet, similar baseline intracellular Ca^{2+} levels and comparable responses to soybean LPI and 20:40 LPI were observed (Fig. 2C). Therefore, subsequent *in vitro* and *in vivo* experiments were only performed with the soybean LPI mix. When comparing *Apoe*$^{-/-}$ and *Apoe*$^{-/-}$*Gpr55*$^{-/-}$ B cell responses in normal diet condition, an increase in intracellular Ca^{2+} after LPI stimulation was only observed in *Gpr55*-expressing *Apoe*$^{-/-}$ cells (Fig. 2D). *Gpr55* deficiency did not affect basal intracellular Ca^{2+} levels, and treatment with the potent B cell stimulus anti-IgM [25,26] resulted in comparably strong Ca^{2+} responses, suggesting that BCR activation by GPR55-independent signals is not compromised in absence of the receptor. Furthermore, human peripheral blood B cells showed a dose-dependent Ca^{2+} response to LPI, indicating a functional LPI-GPR55 signaling pathway in human B cells (Fig. 2E-F).

Gpr55 deficiency disturbs metabolism and drives inflammation

Apoe$^{-/-}$*Gpr55*$^{-/-}$ mice had pronounced metabolic changes, in particular increased body weight compared to aged-matched *Apoe*$^{-/-}$ animals, which was already notable at baseline and consistently evident after 4, 10 or 16 weeks WD (Extended Data Fig. 2A-C). Although plasma cholesterol levels were not significantly different compared to *Apoe*$^{-/-}$ controls at all time points (Extended Data Fig. 2D), the lipoprotein profile analysis at the 4-week time point showed larger VLDL and LDL lipoprotein fractions in *Apoe*$^{-/-}$*Gpr55*$^{-/-}$ mice (Extended Data Fig. 2E). Likewise, the liver total cholesterol was not significantly altered after 4 weeks WD (p=0.086; Extended Data Fig. 2F). Nevertheless, the hepatic qPCR gene expression analysis at the same time point revealed a significant transcriptional upregulation of several metabolic markers, indicating enhanced lipid synthesis, uptake and efflux in *Apoe*$^{-/-}$*Gpr55*$^{-/-}$ mice (Extended Data Fig. 2G). Furthermore, the Oil-Red-O staining analysis of liver sections revealed an enhanced lipid droplet accumulation after 16 weeks WD (Extended Data Fig. 2H-I).

We next investigated the effect of global GPR55 deficiency on vascular and systemic inflammation under conditions of hypercholesterolemia. Compared to *Apoe*$^{-/-}$ controls, *Apoe*$^{-/-}$*Gpr55*$^{-/-}$ mice had a hyper-inflammatory phenotype with an increase in all major circulating and aortic leukocyte subsets (Extended Data Fig. 2J-L); accompanied by an amplified aortic gene expression profile of key pro-inflammatory markers (Extended Data Fig. 2M). Similar effects on plaque development and metabolic changes, as detailed in female mice, were observed in male *Apoe*$^{-/-}$*Gpr55*$^{-/-}$ mice (Extended Data Fig. 3A-C).

Gpr55 deficiency triggers antibody responses

To seek for a possible underlying reason for the excessive pro-inflammatory phenotype and considering that GPR55 is highly expressed by splenic B cells (Fig. 2A), we performed a detailed flow cytometric profiling of B cell populations (Extended Data Fig. 4). Since splenic GPR55 expression was upregulated after 4 weeks WD, but not at the later stage (Fig. 1C), we subsequently focused on this time point for an in-depth profiling of the *Gpr55*-deficient B cell phenotype. The flow cytometric analysis showed a diminished number of splenic B1a counts in *Apoe*$^{-/-}$*Gpr55*$^{+/-}$ mice compared to *Apoe*$^{-/-}$ controls, while B2 marginal zone (MZ) cell counts were increased (Fig. 3A). The most pronounced changes were reductions of splenic germinal center (GC) B cell and PC counts in *Apoe*$^{-/-}$*Gpr55*$^{-/-}$ mice (Fig. 3A). A similar pattern was observed when comparing the relative frequencies among splenic B cell subsets (Fig. 3B-C). B1 cells in *Apoe*$^{-/-}$*Gpr55*$^{-/-}$ mice were shifted to a decreased proportion of the anti-atherogenic B1a subset with increased B1b subset (Fig. 3B-C). Furthermore, there was a decreased proportion of the follicular (FO) subset and increased proportion of the proatherogenic MZ subset (Fig. 3D-E). These flow cytometric data were supported by immunohistological analysis of splenic tissue sections, indicating that B cell follicular and GC areas were less well-defined in mice lacking a functional GPR55 receptor (Fig. 3F).

Despite the reduced splenic PC counts, *Apoe*$^{-/-}$*Gpr55*$^{-/-}$ mice had elevated titers of IgA antibodies and several IgG subclasses (Fig. 3G). The most pronounced increase was detected in IgG2c antibody titers. Comparable increases of IgG subclass titers were observed in male *Apoe*$^{-/-}$ *Gpr55*$^{-/-}$ mice (Extended Data Fig. 3D). In support of the hypothesis that IgG might play a major causal role in the proatherogenic phenotype in absence of GPR55, we found a clear positive correlation between IgG titers and plaque size in *Apoe*$^{-/-}$*Gpr55*$^{-/-}$ mice after 4 weeks WD (Fig. 3H). IgG titers were still higher in *Apoe*$^{-/-}$*Gpr55*$^{-/-}$ mice after 10 and 16 weeks WD, showing that the phenotype was sustained at advanced stages of atherosclerosis (Fig. 3I-J). To clarify whether *Gpr55* deficiency per se affected B cell maturation and antibody secretion, independent of antigens such as OSE arising during hypercholesterolemia, we also quantified antibody titers in the plasma of young mice at 4 weeks of age just after weaning. No differences in antibody titers between young *Apoe*$^{-/-}$ and *Apoe*$^{-/-}$*Gpr55*$^{-/-}$ were detectable, suggesting that an increase of circulating autoantigens during the first weeks of age, likely promoted by pro-atherogenic conditions, promotes the hyperactivated phenotype of B cells when functional GPR55 signaling is lacking (Fig. 3K). Moreover, *Apoe*$^{-/-}$*Gpr55*$^{-/-}$ mice under WD had elevated plasma levels of B cell activating factor (BAFF; Fig. 3L), which is crucial for B cell survival, altogether indicating a hyperactivated B cell response during atherosclerosis in the absence of GPR55 signaling.

The hyperactivated B cell state was linked to an increased number of splenic follicular T helper (Tfh) cells and circulating plasmablasts in *Apoe*$^{-/-}$*Gpr55*$^{-/-}$ mice (Fig. 3 M and N), while long-lived PC counts in the bone marrow were unchanged (Fig. 3O). Taken together, these data suggest an unbalanced humoral response in atherosclerotic mice lacking functional GPR55 signaling, possibly due to disturbed checkpoints controlling the B cell differentiation from a highly proliferative into a specialized antibody secreting cell.

To clarify whether the changes in splenic B2 subsets in absence of functional GPR55 signaling may reflect a defect in B cell maturation, we assessed the lymphoid and B cell progenitor counts of *Apoe*$^{-/-}$*Gpr55*$^{-/-}$ mice after 4 weeks WD compared to corresponding *Apoe*$^{-/-}$ controls. *Apoe*$^{-/-}$ *Gpr55*$^{-/-}$ mice had lower numbers of immature B cells in the bone marrow, and a decrease in the pro-B and activated B cell populations in the spleen; suggesting that GPR55 has an impact at early stages of B cell differentiation (Fig. 3P and Q).

Similar changes in the splenic B cell compartment were observed in female *Gpr55*$^{-/-}$ mice on WT background without *Apoe*$^{-/-}$ deficiency, with increased numbers of B2-MZ B cells and a reduction of PCs (Extended Data Fig. 5A-F). These mice also had increased IgG titers (Extended Data Fig. 5B), accompanied by a decrease in bone marrow long-lived PCs, while circulating plasmablast counts were not significantly different (Extended Data Fig. 5E-F). These data suggest that *Gpr55* deficiency *per se* affects humoral B cell responses even in absence of hypercholesterolemic conditions, even though the phenotype is more pronounced on *Apoe*$^{-/-}$ background combined with atherogenic diet feeding.

Chronic LPI administration does not affect atherogenesis

Next, we asked if the observed *in vitro* effects of LPI on PC maturation could be reproduced *in vivo* by injecting exogenous LPI, and whether it may affect atherogenesis. We used a daily dose of 0.1mg/kg based previously reported *in vivo* doses for testing the effect of LPI injection on liver steatosis,[27] which was in the range of the plasma LPI levels measured in our *Apoe*$^{-/-}$ model. Daily i.p. administration of LPI for 4 weeks in parallel to the atherogenic diet did neither affect the plaque size, nor circulating antibody titers, B cell counts and splenic B cells. Only a slight, yet significant increase in plasma cholesterol compared to the vehicle group was observed (Extended Data Fig. 6B). Although we cannot exclude that the LPI dose was insufficient to affect splenic PC responses and plaque development, or possibly counterbalanced by pro-steatotic effects of LPI[27], another explanation could be that LPI might not be the only endogenous ligand affecting GPR55 signaling *in vivo*.

Bulk RNA-sequencing analysis of splenic B cells

To understand in more detail the role of GPR55 signaling in splenic B cells, we sorted splenic CD19^{+} B cells from 6 *Apoe*$^{-/-}$ and 6 *Apoe*$^{-/-}$*Gpr55*$^{-/-}$ mice after 4 weeks of WD and performed prime-seq, a bulk RNA-sequencing protocol.[28] We found 460 differentially expressed genes (DEGs) between *Apoe*$^{-/-}$ and *Apoe*$^{-/-}$*Gpr55*$^{-/-}$ mice that were enriched in B and T cell activation, cellular response to stress and intracellular signal transduction (Fig. 4A and Extended Data Fig. 7A-B). The main DEGs associated to each GO pathway were validated by qPCR, confirming a decrease of *Fcer2a/CD23* and *Ptprc/LPAP* in *Apoe*$^{-/-}$

Gpr55$^{-/-}$ B cells, together with changes in *Zbtb20*, *Xbp1* and *Bcl6*, which are important transcription factors involved in B cell maturation and PC differentiation (Fig. 4B).[11] To study in more depth the transcriptomic changes linked to altered PC maturation in *Gpr55*-deficient mice, we also performed bulk RNA-sequencing of sorted splenic PC, blood plasmablasts and bone marrow long-lived PC from *Apoe*$^{-/-}$ versus *Apoe*$^{-/-}$*Gpr55*$^{-/-}$ mice. The integration of differentially regulated GO pathways in a chord diagram confirmed that the three populations show overlapping regulated pathways such as B and T cell activation, disrupted Ig production and activated cell stress genes, confirming that B cell maturation and PC function is generally affected by G*pr55* deficiency (Fig. 4C). To further explore the underlying mechanisms caused by the lack of GPR55 signaling, we performed GSEA analysis to identify the immunological molecular signatures altered in our *Apoe*$^{-/-}$*Gpr55*$^{-/-}$ B cell gene set. We found that *Gpr55*-deficiency in B cells was linked to an increased expression of genes necessary for antigen-specific and neutralizing antibody production, supporting the hypothesis that GPR55 in B cells is necessary to control antibody production (FDR q-value=0.0029). Accordingly, *Apoe*$^{-/-}$*Gpr55*$^{-/-}$ B cells downregulated genes negatively involved in antibody production (FDR q-value=0.025). Lack of GPR55 was also associated with a downregulation of genes linked to naïve B cell activation and migration into the light and dark zones of the germinal centers, where B cell clonal expansion, hypermutation, and selection of high-affinity antibody secreting plasma cells occurs (FDR q-value=0.0234). In addition, *Apoe*$^{-/-}$ *Gpr55*$^{-/-}$ B cells downregulated genes involved in Pre-B cell differentiation, signifying that B cell maturation might be affected by *Gpr55* deficiency (FDR q-value=0.0410) (Extended Data Fig. 7C).

In *Apoe*$^{-/-}$ controls, the total splenic G*pr55* expression directly correlated with *Fcer2a/CD23* and *Ptcarp*/LPAP (Fig. 4D-E). B2-FO cells downregulate *Fcer2a*/CD23 expression on the cell surface when they go into memory B cell differentiation.[29] *Ptprc*/LPAP expression was lower in *Apoe*$^{-/-}$*Gpr55*$^{-/-}$ mice, which is in line with previous data reporting that LPAP deficiency is associated with increased MZ B2 cell numbers.[30] Evaluation of transcriptional factors involved in B cell biology revealed lower expression of *Zbtb20* in spleens of *Apoe*$^{-/-}$ *Gpr55*$^{-/-}$ mice, while *Xbp1* expression was 2-fold increased (Fig. 4B). *Zbtb20* is a key player in late B cell differentiation and is highly expressed by GC B cells and PCs.[31] The decreased levels in *Apoe*$^{-/-}$*Gpr55*$^{-/-}$ mice are in line with the lower numbers of GC B cells and disturbed PC differentiation (Fig. 3A).[31] Overexpression of *Xbp1* promotes long-lived PC differentiation and is crucial for switching into secretory cells, releasing large quantities of antibodies, inducing endoplasmic reticulum (ER) remodeling, autophagic pathways, and the induction of the unfolded protein response (UPR).[32] *Ex vivo* stimulation of splenocytes with the GPR55 agonist LPI upregulated CD23 surface expression levels in B cells, with a maximum effect observed after 30 min (Fig. 4F). To substantiate these findings, we compared the CD23 protein expression on splenic B cell subsets after 4 weeks atherogenic diet, confirming reduced surface expression in the total CD19+ and B2 population and in particular B2 FO cells of *Apoe*$^{-/-}$*Gpr55*$^{-/-}$ mice (Fig. 4G).

To further study the role of GPR55 in PC differentiation, we performed additional *in vitro* experiments. Splenic B cells isolated from *Apoe*$^{-/-}$ and *Apoe*$^{-/-}$*Gpr55*$^{+/-}$ mice were stimulated with a cocktail of LPS, IFN-α, IL2, IL4 and IL5 for 72 h to trigger PC differentiation alone or in the presence of the GPR55-agonist LPI or the antagonist CID16020046, respectively.

Co-incubation with LPI resulted in significantly more differentiated PCs compared to cells treated with LPS/IFN-α/IL2/IL4/IL5 alone in B cells isolated from *Apoe*$^{-/-}$ mice, while adding the GPR55 antagonist prevented the LPS/IFN-α/IL2/IL4/IL5-induced induction of PC differentiation (Extended Data Fig. 8A). The effect observed with the GPR55 antagonist without addition of exogenous ligand suggests that pro-inflammatory stimulation leads to endogenous GPR55 ligand production in splenic B cells, which triggers an autocrine receptor activation. The number of differentiated plasmablasts after stimulation with the cytokine cocktail was comparable between *Apoe-/-* and *Apoe-/-Gpr55-/-* B cells. As expected, neither LPI nor GPR55 antagonism affected the cytokine induced plasmablast counts in *Apoe*$^{-/-}$*Gpr55*$^{-/-}$ cells. The effect observed with the GPR55 antagonist without addition of exogenous ligand suggests that pro-inflammatory stimulation leads to endogenous GPR55 ligand production in splenic B cells, which triggers an autocrine receptor activation.

In addition, GPR55 antagonism or genetic depletion significantly augmented the mitochondrial content of *in vitro* differentiated PCs, which may reflect enhanced antibody secretion and cell stress (Extended Data Fig. 8B). We subsequently performed confocal/STED imaging of unstimulated splenic PCs freshly sorted from *Apoe*$^{-/-}$ and *Apoe*$^{-/-}$*Gpr55*$^{-/-}$ mice, which uncovered a different morphology in *Apoe*$^{-/-}$*Gpr55*$^{-/-}$ cells, with enlarged, fused mitochondria and modified actin cytoskeleton (Extended Data Fig. 8C and Supplementary videos).

Furthermore, we used flow cytometry to compare the mitochondrial content of splenic GC B cells, PCs and bone marrow long-lived PCs between *Apoe*$^{-/-}$ and *Apoe*$^{-/-}$*GPR55*$^{-/-}$ mice, which confirmed an increased mitochondrial content in all these subsets (Fig. 4H-J). We may speculate that disturbed Ca^{2+} signaling due to the lack of GPR55 leads to ER stress and increased mitochondrial content.[33] In summary, our findings support a crucial requirement for GPR55 signaling in regulating B cell activation and differentiation into PCs.

B cell-specific *Gpr55* deficiency promotes atherosclerosis

To further address the specific contribution of B cell GPR55 signaling in atherosclerosis, we subsequently used a mixed bone marrow transplantation strategy, employing *μMT* as a model for mice lacking functional B cells, *Gpr55*$^{-/-}$ bone marrow donors on wildtype (WT) background and *Ldlr*$^{-/-}$ mice as recipients. *Gpr55*$^{-/-}$ bone marrow was mixed with *μMT* bone marrow in a 50/50 ratio before transplantation into lethally irradiated *Ldlr*$^{-/-}$ recipients (Fig. 5A). The B cell-specific deficiency was validated after 6 weeks recovery by qPCR of sorted circulating B cells, while T cells and myeloid cells exhibited normal expression levels of *Gpr55* (Fig. 5B). At the end point following recovery and 10 weeks WD feeding, the metabolic effects observed in *Apoe*$^{-/-}$*Gpr55*$^{-/-}$ mice were lost, as we did not observe changes in body weight between groups. We even observed a slightly decreased plasma cholesterol in B cell-specific *Gpr55*-deficient mice compared to their respective controls (Fig. 5C-D).

Mice with B cell specific *GPR55* deficiency developed larger plaques compared to control mice transplanted with a mixture of WT/*μMT* bone marrow (Fig. 5E-F) and had less splenic B1 cells, MZ B cells and FO B2 cells, while PC counts were elevated (Fig. 5G). The distinct profile in splenic B cell subsets of B cell-specific compared to global *Apoe*$^{-/-}$*Gpr55*$^{-/-}$

mice indicates that the observed phenotype in global knockouts was not only due to B cell-dependent effects, but also modulated by T cell responses, such as Tfh interactions. Interestingly, we also observed changes in B cell CD23 expression levels, but with different B cell subsets affected compared to global *Apoe*$^{-/-}$*Gpr55*$^{-/-}$ mice. In the chimeras with B cell specific deficiency, the CD23 expression level was lower in B1, B1b and B2 MZ cell subsets (Fig. 5H), suggesting a B cell-intrinsic GPR55-dependent regulation of CD23 expression. Assessment of circulating antibody titers revealed slightly reduced plasma IgM titers, while IgGs were increased in B cells-specific *Gpr55*-deficient mice (Fig. 5I), which is in line with the proatherogenic phenotype. In particular, we observed significantly increased plasma titers of MDA-LDL-specific IgGs, which points to an involvement of specific responses to OSE under hypercholesterolemic conditions (Fig. 5J).

Adoptive transfer of *Gpr55*$^{-/-}$ B cells fuels atherosclerosis

To substantiate the crucial importance of functional B cell GPR55 signaling in atherosclerosis, we performed an adoptive transfer experiment by injecting *Gpr55*$^{-/-}$ B cells into *Apoe*$^{-/-}$ mice. For this purpose, we treated *Apoe*$^{-/-}$ mice with a B cell depleting antibody cocktail and validated the depletion efficiency in blood and spleens in a pilot experiment (Fig. 6A-B). Next, we subjected *Apoe*$^{-/-}$ mice to the same depletion protocol before transferring WT or *Gpr55*$^{-/-}$ B cells. All experiments were performed with female recipients and cells from female donors. The adoptive transfer of *Gpr55*$^{-/-}$ B cells was sufficient to trigger an increase in plasma IgG levels and plaque size after 4 weeks of WD compared to the control group receiving WT B cells, without effects on body weight, plasma cholesterol and IgM levels (Fig. 6C-H). Moreover, the analysis of splenic B cell numbers revealed a decrease in almost all B cell subsets in *Gpr55*$^{-/-}$ compared to WT B cell recipients, including the B1a, total B2 and PC subsets (Fig. 6I), suggesting that *Gpr55*$^{-/-}$ B cell transfer was sufficient to confer an antibody-associated phenotype with disturbed splenic B cell differentiation.

Discussion

Our study provides previously unknown insights into the contribution of the lipid receptor GPR55 in atherosclerosis. Its role appears to be complex, ranging from metabolic to B cell specific effects. Mice with B cell-specific *Gpr55* deficiency had reduced plasma cholesterol levels, which may suggest that *Gpr55* deficiency in B cells promotes lipid removal e.g. by increasing their surface expression of lipid binding receptors,[34] which is masked by the pro-steatotic effects in the global knockouts. Our liver metabolic data in the global *Apoe*$^{-/-}$*Gpr55*$^{-/-}$ mice are somewhat controversial to recent findings in hepatocytes, where a pro-steatotic function of GPR55 signaling was documented by stimulation with the synthetic agonist O-1602, an effect that was reversed by the GPR55 antagonist CID16020046.[35] These discrepancies might be explained in part by the fact that O-1602 also binds to GPR18 and different dietary conditions.[36]

The finding that GPR55 is highly expressed by splenic PCs suggests a central role for GPR55 in this immune cell subset. Yet, our data support a more pleiotropic implication of GPR55 in B cells, affecting bone marrow differentiation, activation, germinal center

formation and PC differentiation. GPR55 signaling exerts an atheroprotective effect in B cells, while the lack of GPR55 promotes an uncontrolled T and B cell interaction, leading to increased Tfh and circulating plasmablast counts, together with elevated plasma BAFF levels, thereby cumulating in an excessive IgG production. Many genes and pathways involved in B and T cell activation, cellular response to stress and intracellular signal transduction were differentially regulated in *Gpr55* deficient B cells. Exploration of the Molecular Signatures Database (MSigDB) collection of immunologic signature gene sets highlighted the importance of GPR55 expression and signaling in antigen-specific and neutralizing antibody production and naïve B cell activation and migration into the GC light and dark zones, where B cell clonal expansion, hypermutation, and selection of high-affinity antibody secreting PCs occurs.[10] Among the downregulated genes in *Apoe*$^{-/-}$*Gpr55*$^{-/-}$ B cells, *Fcer2a/CD23* and *Ptprc*/*LPAP* are positively correlated with *Gpr55* expression. Previous studies using CD23 knockout mouse models suggested that CD23 is not critical for B and T cell maturation, but plays a regulatory function in the adaptive immune response.[37] Liu *et al.* demonstrated that CD23 negatively controls BCR signaling by inhibiting actin-mediated BCR clustering and B cell morphological changes.[29] Moreover, a link between CD23 expression and IgG antibody response has been proposed.[38] In particular, overexpression of CD23 resulted in significantly decreased IgG antibody responses. Hence, we may speculate that the decreased expression of CD23 in absence of GPR55 and thus lack of inhibitory signal for BCR signaling and IgG responses may contribute to the observed phenotype in our model. MZ and FO B cells are known to downregulate CD23 after undergoing isotype switch and memory B cell differentiation. In mice lacking CD23, antigen stimulation resulted in increased BCR clustering and F-actin at the cell surface[29], which phenocopies our observations in the *Apoe*$^{-/-}$*Gpr55*$^{-/-}$ mice. TThe different PC profile in mice with B cell specific *Gpr55* deficiency is likely related to the fact that GPR55 signaling in T cells is preserved. In addition, given that neutrophils also express relatively high levels of the receptor we speculate that enhanced neutrophil inflammatory responses in absence of global GPR55 signaling lead to a more pronounced systemic inflammatory response and strong BCR activation. The plasma cell phenotype in B cell-restricted *Gpr55* deficiency may be linked to antigen-independent constitutive BCR signaling, which promotes spontaneous plasma cell differentiation. Less is known regarding *Ptprc*/LPAP in B cells. *In vitro* stimulation of *Ptprc* mutant B cells led to normal differentiation into plasmablasts, but the cells failed to downregulate B220 expression, albeit it did not affect their functionality.[39] The altered mitochondrial and actin cytoskeleton structure in *Gpr55* deficient PCs is in agreement with an enhanced activation state. Activated B cells exposed to high levels of BAFF increased glucose uptake and mitochondrial mass, resulting in increased glycolysis and oxidative phosphorylation.[40,41] Although the mitochondrial dynamics in PCs have not been studied in detail, it is likely that IgG secretion in these cells is linked to increased metabolic rates and induces cellular stress responses.[40,42–44] The observed Ca^{2+} influx in response to LPI stimulation may play an important role in the regulation of cellular responses in PCs, including mitochondrial physiology and Ig production.[45] Lack of GPR55 signaling may reduce intracellular/ER Ca^{2+} stores, contributing to a defective BCR effector pathway activation. However, our *in vitro* experiments did not reveal changes in basal Ca^{2+} levels nor in response to the potent Ca^{2+} stimulus anti-IgM.

The role of LPI in B cell GPR55 signaling and atherogenesis remains incompletely understood. *In vitro*, LPI stimulated B cell maturation into PCs, which was inhibited when antagonizing GPR55. The effect was observed without addition of exogenous LPI, suggesting endogenously produced ligands in response to the inflammatory stimulation. *In vivo*, LPI treatment did neither affect the plaque size nor splenic B cell counts. Only a significant increase of plasma cholesterol levels was observed in LPI- compared to vehicle-treated mice. The reason for the lack of effects on atherosclerosis might be multifold. Given that LPI injection resulted in significantly elevated plasma cholesterol levels, which is in line with data reporting that 7 days of LPI injection induced liver steatosis,[27] we may speculate that the pro-steatotic effects counterbalanced a possible atheroprotective phenotype. Moreover, LPI might not be stable enough to affect B cell differentiation *in vivo*. In addition, the local LPI release in splenic microdomains might be important to specifically act on plasmablasts in the red pulp or plasma cells in germinal centers. A better approach to address the *in vivo* relevance might be to block the enzymatic pathways involved in its degradation, which would require specific enzyme inhibitors to block LPI metabolic pathways. It is also possible that other endogenous GPR55 ligands (e.g. palmitoylethanolamide) contribute to B cell GPR55 signaling.[46] Furthermore, LPI effects might be limited to atherogenesis, in line with the early peak of splenic *Gpr55* and *Ddhd1* expression as well as plasma LPI levels. This might be linked to the increase of circulating atherosclerosis-related antigens during onset of diet thereby activating dendritic cells to release LPI, while this response is dampened in the more chronic disease state.

Another unresolved question remains the role of GPR55 in other immune subtypes. Our gene expression analysis of sorted splenic immune cell subsets indicates a strong GPR55 expression in T cells, which deserves further investigation in subsequent studies. The fact that GPR55 signaling in T cells is preserved may contribute to the observed differences in B cell subsets and antibody titers between the global and B cell specific deficiency models. Our study employing global and B cell specific *in vivo* approaches based on mixed bone marrow chimeras and adoptive B cell transfer at least confirms that GPR55 signaling in B cells crucially regulates atherosclerosis.

To conclude, our experimental *in vivo* and *in vitro* data, together with the confirmation of GPR55 expression and correlation with disease stage in human atherosclerosis, strongly support an implication of GPR55 in atherosclerosis. We uncovered a previously undescribed role for GPR55-LPI signaling in PC differentiation, at least *in vitro*. The transcriptomic signature and phenotype of *Gpr55*-deficient B cells supports that GPR55 provides a negative signal for BCR signaling with most prominent effects on CD23 regulation. However, the pleiotropic *in vivo* effects of *Gpr55* deficiency on B cell bone marrow differentiation, activation, GC formation and PC differentiation suggest a more general role of the receptor in the B cell lineage, which cannot be attributed to a single molecular mechanism. Orphan receptors such as GPR55, which are activated by bioactive lipid mediators may represent an interesting therapeutic target to be further explored in the context of chronic inflammatory diseases such as atherosclerosis and beyond.

Methods

Global *Gpr55*-deficiency mouse model of atherosclerosis

Gpr55$^{-/-}$ mice on C57BL/6J wildtype (WT) background were purchased from the European Mouse Mutant Archive (EM:02355), genotyped as previously reported[47] and backcrossed with *Apoe*$^{-/-}$ mice (strain #002052, The Jackson Laboratory). Male and female *Apoe*$^{-/-}$ and *Apoe*$^{-/-}$ *Gpr55*$^{-/-}$ mice aged 7 to 9 weeks were fed with Western diet (WD; 0.20% cholesterol, Ssniff, TD88137) for either 4, 10 or 16 weeks. Female C57BL/6J and *Gpr55*$^{-/-}$ mice on C57BL/6J wildtype were used at 6 to 8 weeks of age. At the end point, mice were anesthetized with ketamine/xylazine, and blood was obtained via cardiac puncture. Heart, aorta, spleen, femurs, and livers were harvested after PBS perfusion. All animal experiments were approved by the local Ethics committee (District Government of Upper Bavaria; License Number: 55.2-1-54-2532-111-13 and 55.2-2532.Vet_02-18-114) and conducted in accordance with the institutional and national guidelines and following the ARRIVE guidelines. Animals were housed in individual ventilated cages in groups of 4 to 6 mice in 12-hour light–dark-cycle, air-conditioned (23°C and 60% relative humidity) with free *ad libitum* access to food pellets and tap water. Sample size for the experiments was selected for achieving an *a priori* 85% statistical power for biologically significant difference (d=0.8).

B cell-specific *Gpr55*-deficient bone marrow chimeras

Female *Ldlr*$^{-/-}$ mice (strain #:002207, The Jackson Laboratory), female *Gpr55*$^{-/-}$ mice on WT background and B cell-deficient (*μMT*) female mice (strain # 002288, The Jackson Laboratory) aged 6–8-weeks at the start of experimental regimes were used. *Ldlr*$^{-/-}$ mice were irradiated with 8 Gy gamma-radiation and reconstituted with 2×10^6 mixed bone marrow cells consisting of 50% *μMT* marrow and 50% *Gpr55*$^{-/-}$ or WT marrow, respectively. After irradiation mice were recovered for 6 weeks and then subjected to WD feeding for 10 weeks. After the 6-week-recovery time point, tail vein blood was collected to assess the transplantation efficiency. At the end point, blood and organs were collected as described above.

Chronic lysophosphatidylinositol (LPI) treatment

Age- and weight-matched littermate female *Apoe*$^{-/-}$ mice were randomly divided into two groups to receive daily intraperitoneal (i.p.) injections of 0.1 mg/kg LPI (L-α-lysophosphatidylinositol sodium salt from soybean; Sigma-Aldrich, # 62966) or vehicle (0.05% Tween 80, 0.1% DMSO in saline), respectively. Both groups were fed with WD for 4 weeks. At the end point, blood and organs were collected as described above.

Adoptive transfer of B cells

B cells were isolated from spleens of WT and *Gpr55*$^{-/-}$ female mice and enriched with a B cell isolation kit (Miltenyi Biotec MACS). The purity was 97±1.2%. B cells were intraperitoneally (i.p.) injected into B cell-depleted female *Apoe*$^{-/-}$ mice (1×10^6 cells) treated three days prior to the adoptive B cell transfer with a cocktail of the following antibodies: B220 (clone RA3.3A1/6.1, ref: BE0067), CD19 (clone 1D3, Ref: BE0150) and CD22 (clone Cy34.1, BE0011), and 48 h later anti-rat kappa (clone TIB216, Ref: BE0122, all antibodies

from BioXCell; 150 μg i.p. per antibody). To test the B cell depletion efficiency, some mice were treated with a depletion antibody cocktail or isotype (IgG1, BE0083, BioXCell) and euthanized 72 h after the first injection to measure leukocyte counts in the blood and spleen by flow cytometry. At the end point, blood and organs were collected as described above.

Human material

The permission to collect human carotid atherosclerotic biospecimens for the Munich Vascular Biobank was approved by the local Hospital Ethics Committee (Ethikkommission der Fakultät für Medizin der Technischen Universität München, Munich, Germany). All patients provided their written informed consent. Human carotid artery plaques were harvested during carotid artery endarterectomy (CEA) surgery, transported to the laboratory and snap frozen. Carotid tissue with an unstable/ruptured or stable plaque phenotype, depending on symptoms of plaque instability and the size of the fibrous cap (cutoff of 200 μm)[48,49] was cut in ~50mg pieces on dry ice. The patients' characteristics are summarized in Extended Data Table 1. The tissue homogenization was performed in 700 μl Qiazol lysis reagent and total RNA was isolated using the miRNeasy Mini Kit (Qiagen, Netherlands) according to manufacturer´s instruction. RNA concentration and purity were assessed using NanoDrop. RIN number was assessed using the RNA Screen Tape (Agilent, USA) in the Agilent TapeStation 4200. Next, first strand cDNA synthesis was performed using the High-Capacity-RNA-to-cDNA Kit (Applied Biosystems, USA), following the manufacturer's instructions. Quantitative real-time PCR was performed in 96 well plates with a QuantStudio3 Cycler (Applied Biosystems, USA), using TaqMan Gene Expression Assays (ThermoFisher, USA) for detection of the following expressed genes: *RPLPO* (Hs99999902_m1), *GPR55* Hs00271662_s1).

Cholesterol and triglyceride measurement

Liver tissue (50-70 mg) was homogenized in 500 μl of 0.1 % NP-40 in PBS using a bead mill Tissue Lyser (Qiagen) and centrifuged for 2 min at 3000 x g to remove the insoluble material. Total plasma cholesterol and triglyceride concentrations were quantified in murine plasma and liver homogenates using colorimetric assays (CHOD-PAP and TAG-PAP Roche) according to the manufacturer's protocol.

Lipoprotein profile analysis

Plasma samples were subjected to fast-performance liquid chromatography (gel filtration on a Superose 6 column; GE Healthcare, Chicago, IL). Different lipoprotein fractions (VLDL [very-low density lipoprotein], LDL, and HDL [high-density lipoprotein]) were separated and evaluated based on flow-through time.

LPI analysis by liquid chromatography-tandem mass spectrometry

Plasma samples were allowed to thaw on ice water, and 50 μl aliquots were transferred to 1.5 ml centrifugation tubes. After adding 300 μL of ice-cold ethyl acetate/hexane (9:1, v/v) containing the deuterated LPI as internal standards, tubes were vortexed and centrifuged for 15 minutes at 20000 x g at 4° C. The upper organic phase was removed, evaporated to dryness under a gentle stream of nitrogen at 37° C, and reconstituted in 50 μl acetonitrile/

water (1:1, v/v). Plasma concentrations of LPI were determined by liquid chromatography-multiple reaction monitoring and normalized to the total volume of supernatant.[50] Only LPI 20:4 was targeted and quantified, while other LPI species with other fatty acyl composition such as LPI16:0, LPI 18:0 were excluded based on retention time and transition of precursor m/z to fragment m/z. Isoforms of LPI20:4 like sn1/sn2 cis/trans or position of double bond within the LPI 20:4 composition were not detected/included.

Histological studies

Mouse hearts and livers were isolated after perfusion with PBS and frozen in Tissue-tek (Sakura Finetek). Aortic roots were cut in 4-μm and liver sections at 5-μm thick serial cryosections. The sections were stained with Oil-Red O for total plaque and lipid analysis and aortic roots were also stained with Masson´s trichrome for collagen in accordance with the guidelines for experimental atherosclerosis studies by the American Heart Association.[51] Lesion size was analyzed in a blinded manner and quantified in 8 sections per heart, separated by 40 μm from each other, to cover the entire aortic root. For conventional immunofluorescence, aortic root sections were fixed for 5 min with 4% formalin and blocked for 1 h at room temperature (RT) with blocking buffer (PBS with 1% bovine serum albumin (BSA)). Then the slides were incubated with Mac2 primary antibody overnight at 4° C for macrophage staining followed by anti-rat-AF488 for 2 h at RT, and nuclear staining (Hoechst33342) for 5 min. Images were acquired using a Leica DM6000B fluorescence microscope equipped with a digital camera (DFC365, Leica). The Leica Application Suite LAS V4.3 software or ImageJ software were used for the lipid, plaque and macrophages quantification. Splenic cryosections of 10-μm thickness were fixed for 5 min with 4% formalin and blocked for 1 h at RT, then stained with directly conjugated antibodies overnight at 4° C. PNA-FITC (1:100) for GC B cells, IgM-AF647 (1:250) for MZ B cells and memory B cells, CD23-AF594 (1:100) for FO B cells, and Hoechst33342 for the nuclei staining. Digital images were acquired using a three-dimensional confocal laser scanning microscope (CLSM; Leica SP8 3X) equipped with a 100xNA1.40 oil immersion objective (Leica).

In situ hybridization for *Gpr55*

GPR55 cells was detected by *in situ* hybridization (FISH) by using a murine *Gpr55* probe (VB6-3216575, Affymetrix). The splenic sections were cut and collected in RNAse free slides. The sections were prefixed in 4% PFA for 5 min at RT and washed 3 times with PBS for 5 min. The tissue sections were treated with pre-warmed 10 μg/ml proteinase K (diluted in PBS) for 5 min at RT, followed by post-fixing with 100% ethanol for 1 min. After washing with PBS, the sections were transferred to an RNAse free chamber. The ViewRNA™ Cell Plus Assay-Kit (Invitrogen) was used for target probe hybridization by incubating the sections at 40° C for 2 h. The hybridization probe was mixed with probe set diluent to a final concentration of 5 μg/ml. Following the hybridization step, the sections were washed and a signal amplification was performed by incubating with the pre-amplifier mix for 30 min at 40° C, washing and incubating with the amplifier mix for 1 h at 40° C. After washing, the sections were incubated for 1 h at 40° C with the working label probe mix. Following the in-situ hybridization for the *Gpr55* probe, the sections were washed,

incubated with blocking buffer at RT for 1 h and stained with PNA-FITC, IgM-AF647 and CD23-AF594 antibodies as described above.

Flow cytometry

Splenic single cell suspensions were obtained by mashing the spleens through a 70-μm cell strainer. Femurs were centrifuged at 10,000 x g for 1 min after exposure of the distal metaphysis to collect the bone marrow cells. Splenic, bone marrow and blood erythrocytes were lysed with ammonium-chloride-potassium (ACK, NH_4Cl (8,024 mg/l), $KHCO_3$ (1,001 mg/l) $EDTA.Na_2{\cdot}2H_2O$ (3.722 mg/l) buffer for 10 min at RT. For staining of leukocytes infiltrated into the aorta, the vessels were excised from the aortic arch to iliac bifurcation, and digested with collagenase IV and DNase I at 37° C at 750 rpm for 40 min[52] and filtered through a 30-μm cell strainer. Blood, splenic, bone marrow, and aortic single cells were blocked for 5 min with Fc-CD16/CD32 antibody and then stained for 30 min in the dark at 4° C with antibodies (Supplementary Table 1) to identify cell subsets. After gating for living singlets and $CD45^+$, the $CD11b^+$ myeloid subsets were further gated as following: $CD115^+Ly6G^-$ (monocytes), $F4/80^+$ (macrophages), $CD115^-$ $Ly6G^+$ (neutrophils). The $CD11b^-$ lymphoid population was divided into $CD3^+$ (T cells) and $CD19^+$ (B cells). B cell subsets were further identified as $B220^{low}CD23^-CD5^+$ (B1a), $B220^{low}CD23^-CD5^-$ (B1b), $B220^{high}CD23^-IgM^+$ (MZ), $B220^{high}CD23^-IgM^{int}IgD^+$ (FO), $B220^{high}CD23^+IgM^{int}PNA^+GL7^+$ (GC) (Extended Data Fig. 4). PCs were gated as $CD19^-CD138^+CD23^-IgM^-IgD^-$ and splenic Tfh were gated as $CD3^+CD19^-CXCR5^+PD1^+$. The circulating plasmablasts were identified as $CD19^+CD38^+CD138^+$ and long-lived bone marrow PCs as $CD19^-CD138^+$. Lymphoid and B cell progenitor populations were gated as follows: lin-(CD3-CD11b-B220-Gr1-Ter119-) and CD127+ (CLP), lin-B220+CD19-CD43+ (pre-proB), lin-B220+CD19+CD43+ (proB), lin-CD19+CD43-CD24+CD127+ (pre-B), lin-CD19+IgM+ (immature B cells), and lin-CD19+CD43-CD24+CD127-IgD+ (activated B cells).

For mitochondrial staining in splenic and bone marrow B cells, the cells were incubated with prewarmed (37° C) staining solution containing MitoTracker (ThermoFisher) at a concentration of 50 nM for 30 min. After removing the mitochondrial staining solution by centrifugation, the cells were stained with specific antibodies to identify the different B cell subpopulations. Flow cytometry data were acquired on a BD FACSCanto II flow cytometer (BD Biosciences) or Fortessa LSR (BD Biosciences) and analyzed with FlowJo v10.2 software (Tree Star, Inc).

Flow cytometric sorting of splenic B cells

Single cell suspensions obtained from *Apoe*$^{-/-}$ and *Apoe*$^{-/-}$*Gpr55*$^{-/-}$ spleens were sorted using a BD FACSAria III Cell Sorter (BD Biosciences) as $CD19^+$ total B cells or $B220^{high}CD23^+IgM^{int}PNA^+GL7^+$ GC cells. Circulating plasmablasts were gated as $CD19^+CD38^+CD138^+$, and bone marrow long-lived PCs as$CD19^{-/-}CD138^+$. The sorted cells were deep frozen in 2x TCL buffer plus (Qiagen) plus 1% beta-mercaptoethanol.

RNA-sequencing and analysis

Sorted cells were used to perform bulk RNA-sequencing using the prime-seq protocol that can be found on protocols.io (dx.doi.org/10.17504/protocols.io.s9veh66).[28] Briefly, 10000 sorted cells were lysed in 100 μL of RLT+, 1% beta-mercaptoethanol and 50 μL of lysate was used for RNA-sequencing. In case that less than 10,000 cells could not be obtained, all sorted cells were used. The samples were proteinase K and DNase I digested and then cDNA synthesis was performed using uniquely barcoded oligodT primers. Samples destined for the same library were pooled and pre-amplification was then performed using 11-14 cycles, depending on the initial input per library. The cDNA was quantified using the PicoGreen dsDNA assay kit (Thermo Fisher, P11496) and qualified using the Bioanalyzer HS DNA chip (Agilent, 5067-4626). Libraries were then constructed with the NEB Next Ultra II FS kit (E6177S, NEB) using the prime-seq specifications. The libraries were quantified and qualified using the HS DNA chip on the Bioanalyzer and sequenced on an Illumina Hiseq 1500 at an average depth of 12.7 million reads per sample. The reads were demultiplexed using deML and then filtered, mapped to the mouse genome (mm10, GRCm38), and counted using zUMIs (version 2.5.5) with STAR.[53] Differential gene expression analysis was performed using DESeq2 and then the characterization of the molecular functions or pathways in which differentially expressed genes (DEGs) are involved was performed using gene set enrichment analysis (GSEA). In addition, GSEA software was used to find immunological gene set annotations by using the ImmuneSigDB subset (C7) Molecular Signature Database (MSigDB) [54–57]. Other resources used were Gene Ontology, Bioconductor, Gorilla and DAVID.

Quantitative real-time polymerase chain reaction

Aortas, sorted leukocytes and splenic B cell subsets were homogenized and lysed for extraction of total RNA (peqGold Trifast and Total RNA kit, Peqlab). After reverse transcription (PrimeScript RT reagent kit, Clontech), real-time PCR was performed with the 7900HT Sequence Detection System (Applied Biosystems) using the KAPA PROBE FAST Universal qPCR kit (Peqlab). Primers and probes were purchased from Life Technologies. Target gene expression was normalized to *Hprt* (hypoxanthine-guanine phosphoribosyltransferase) and presented as relative transcript level ($2^{-\Delta\Delta Ct}$). For comparison of *Gpr55* expression, *Gapdh* (glyceraldehyde-3-phosphate dehydrogenase) was used as additional housekeeping control for normalization (Supplementary Table 2).

Digital droplet PCR

For performing the digital droplet-PCR (ddPCR) we prepared the reaction mixture by combining a 2x ddPCR Mastermix (Bio-Rad), 20x primer, and probes (final concentrations of 900 and 250 nM, respectively; Integrated Data Technologies) and template in a final volume of 20 μl (Supplementary Table 3). Then, each ddPCR reaction mixture was loaded into the sample well of an eight-channel disposable droplet generator cartridge (Bio-Rad). A volume of 60 μl of droplet generation oil (Bio-Rad) was loaded into the oil well for each channel. The cartridge was placed into the droplet generator (Bio-Rad), and the droplets were collected and transferred to a 96-well PCR plate. The plate was heat-sealed with a foil seal, placed on the thermal cycler and amplified to the endpoint (40 cycles). After PCR, the

96-well PCR plate was loaded on the droplet reader (Bio-Rad). Analysis of the ddPCR data was performed with QuantaSoft analysis software (Bio-Rad).

Immunoglobulin measurement in plasma

To measure Ig isotypes and subclasses in plasma, the Antibody Isotyping 7-Plex Mouse ProcartaPlex™ Panel was performed with a MAGPIX luminex reader (ThermoFisher). For total IgG and IgM quantification, single ELISA kits were used (ThermoFisher). Anti-MDA specific IgGs were measured by coating MaxiSorp plates (NuncTM, city, Roskilde, Denmark) with purified, mouse-derived delipidated apolipoprotein MDA for 1 h at 37° C. After being washed, all wells were blocked for 1 h with 2% BSA in a PBS at 37° C. Mouse samples were also added to a non-coated well in order to assess individual non-specific binding. After washing, 50 μl/well of the alkaline phosphatase-conjugated anti-mouse IgG was added (Sigma-Aldrich), it was diluted at 1:1000 in a PBS/BSA 2% solution, and this was added and incubated for 1 h at 37° C. After washing, phosphatase substrate p-nitrophanylphosphate disodium (Sigma-Aldrich) dissolved in a diethanolamine buffer (pH 9.8) was added and incubated for 30 min at 37° C. Optical density (OD) was determined at 405 nm (Filtermax 3, Molecular DevicesTM, San Jose, CA) and each sample was tested in duplicate. Corresponding non-specific binding was subtracted from mean OD for each sample.

In vitro PC differentiation

Splenic B cells were isolated from *Apoe*$^{-/-}$ and *Apoe*$^{-/-}$*Gpr55*$^{-/-}$ mice mice by meshing the spleen and subsequent entrichment for CD19^{+} cells using a Miltenyi kit. For PC *in vitro* differentiation, the isolated B cells were seeded in 24-well plates and treated with a cocktail of LPS (0,5 ng/ml), IFN-α (2 ng/ml), IL2 (5 ng/ml), IL4 (5 ng/ml), and IL5 (2 ng/ml) for 7 days, adding fresh medium with the stimulation cocktail every second day, based on an optimized protocol according to previous publications.[58,59] In some conditions, the stimulation cocktail was combined with LPI (Sigma-Aldrich #62966) or CID16020046. After 7 days, cells were collected and used for flow cytometric analysis of the total number of PCs, gated as viable single CD45^{+}CD11b^{-} CD19^{+}CD138^{+} cells. For mitochondrial staining, the cells were incubated with prewarmed (37° C) staining solution containing MitoTracker (ThermoFisher) at a concentration of 50 nM for 30 min. After removing the mitochondrial staining solution by centrifugation, the cells were stained with specific antibodies to identify the PCs. Flow cytometry data were acquired on a BD FACSCanto II flow cytometer (BD Biosciences) and analyzed with FlowJo v10.2 software (Tree Star, Inc).

Confocal/STED imaging of splenic PCs

Splenic B cells were isolated from *Apoe*$^{-/-}$ and *Apoe*$^{-/-}$*Gpr55*$^{-/-}$ mice, seeded into glass-bottom chamber 8-well slides (Ibidi) and differentiated into PCs as described above. We stained the mitochondria following the above described protocol, and then the slides were subsequently stained with F-actin for 30 min at RT, followed by incubation for 5 min with Hoechst33342 (ThermoFisher Scientific) and embedded with ProLong Diamond Antifade Mountant (ThermoFisher). Digital images were acquired using a three-dimensional CLSM combined with STED (Leica SP8 3X) equipped with a 100xNA1.40 oil immersion objective (Leica). Optical zoom was used where applicable. For fluorescence excitation, a UV laser

(405 nm) was used for excitation of Hoechst and a tunable white light laser for selective excitation of other fluorochromes (Alexa488, Alexa594 and Alexa647). Depletion was performed at 592 nm and 775 nm for AlexaFluor488 and AlexaFluor594, respectively. Images were collected in a sequential scanning mode using hybrid diode detectors to maximize the signal collection and reduce the background noise and overlap between the channels. All data were acquired in three dimensions and voxel size was determined according to Nyquist sampling criterion. Image reconstructions were performed using the LAS X software package v.3.0.2 (Leica) and deconvolution was applied in combination with the Huygens Professional software package v.19.10 (Scientific Volume) using the unsupervised CMLE (for CLSM) algorithm. Visualization of 3D images is provided as a video showing the merged fluorescent channels from different visual perspectives (Supplemental videos). To this end, 3D rendering was performed using the LAS X 3D software and visual perspective was automatically selected by the software to provide the best visualization.

Ca^{2+} assay and CD23 stimulation

Ca^{2+} responses and CD23 surface expression was measured in murine blood isolated from female baseline (normal diet fed) WT mice, baseline or 10 weeks WD fed *Apoe*$^{-/-}$ mice and baseline *Apoe*$^{-/-}$*Gpr55*$^{-/-}$ mice. Briefly, the cells were stained with an antibody cocktail to identify cell subpopulations, washed and then incubated with FLIPR, Calcium 5 Assay Kit (Molecular devices) for 1 h at 37° C. After stimulation with soybean LPI (Sigma-Aldrich #62966) or pure 20:4 LPI (Sigma-Aldrich #850105P) for 30 seconds, the samples were immediately analyzed by flow cytometry to determine the mean fluorescence intensity (MFI) of intracellular Ca^{2+}. The CD23 surface expression was measured after 10 to 60 min LPI stimulation.

Statistical Analysis

Statistical analyses were performed using GraphPad Prism version 9.1.1 software (GraphPad Software, Inc., San Diego, CA, USA). To test for Gaussian distribution, D'Agostino Pearson omnibus or Shapiro–Wilk normality test was applied. Outliers were determined by Grubbs' test (alpha 0.05). After testing homogeneity of variances via *F* test, Student's *t* test was used for normally distributed data with equal variances. For heteroscedastic data, Welch correction was applied. Mann–Whitney *U* test was performed if normality test failed. Comparisons among >2 groups by one-or two-way ANOVA with Tukey post hoc test or Kruskal–Wallis test with Dunn post hoc test, as indicated in each figure legend. Bivariate correlations involving *Gpr55* expression, plaque area or plasma IgG were analyzed by Spearman's rank correlation test, to avoid assumptions on data distribution. All data are shown as mean ± SEM. A 2-tailed $p<0.05$ was considered statistically significant.

Europe PMC Funders Author Manuscripts

Extended Data

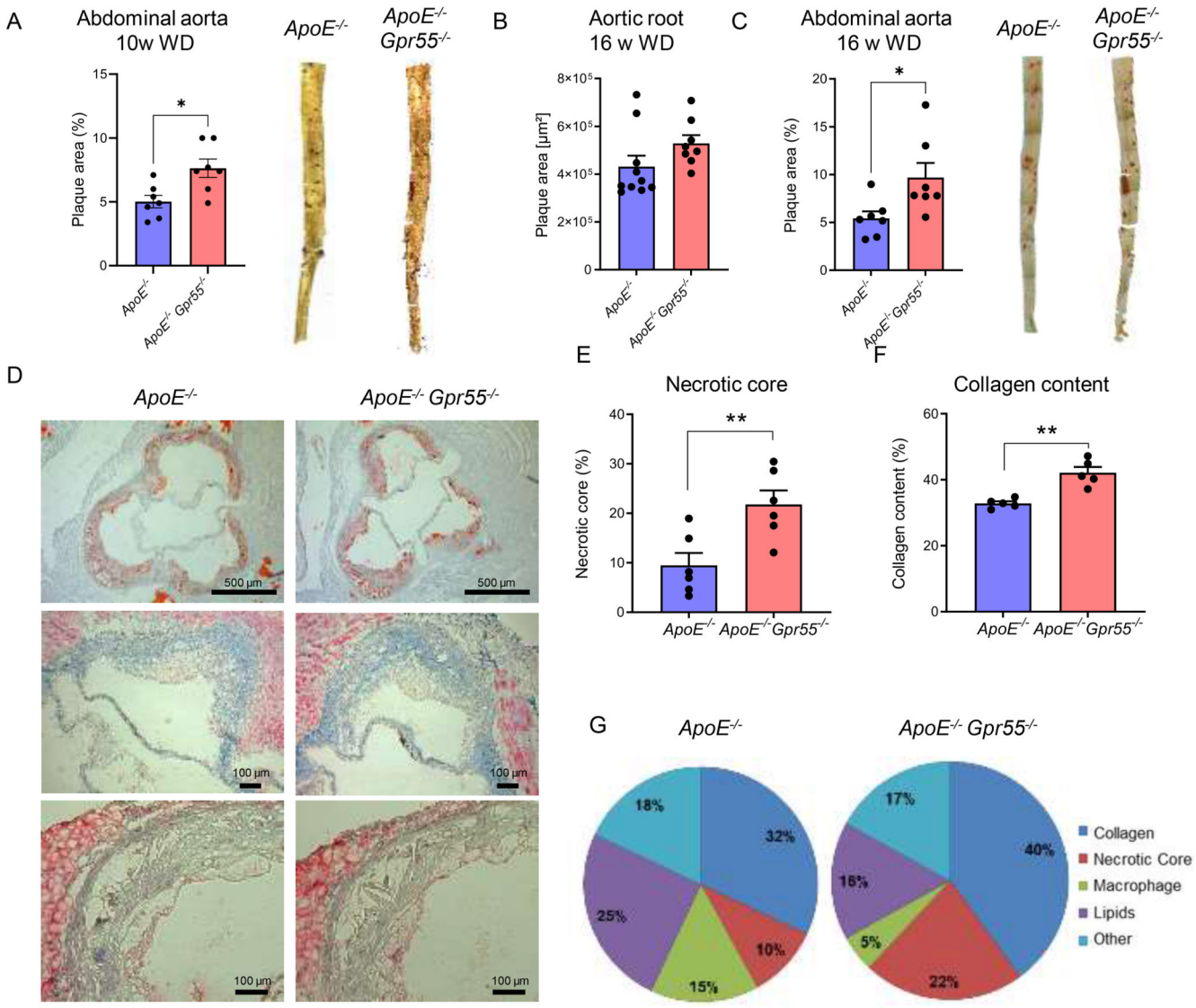

Europe PMC Funders Author Manuscripts

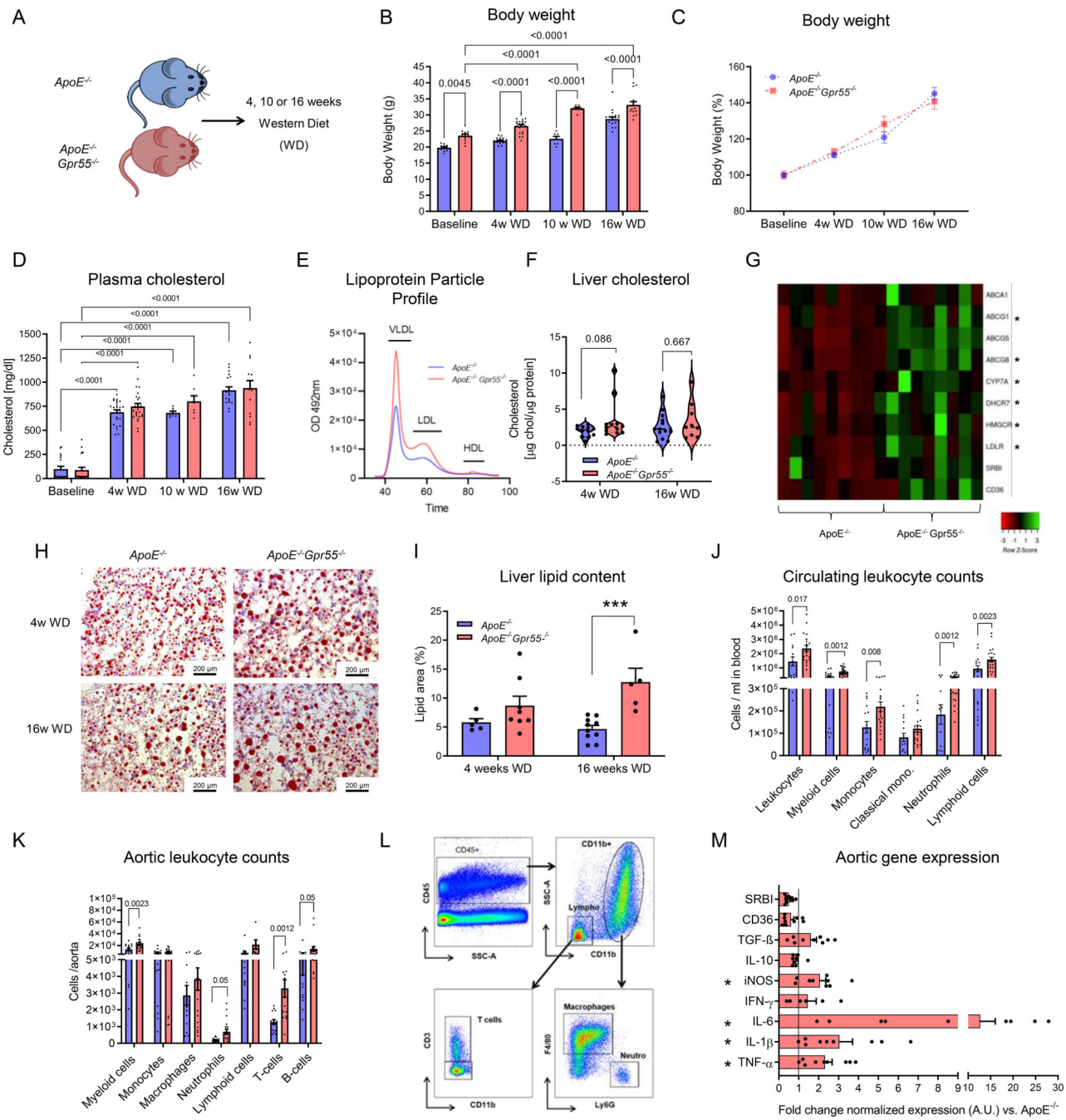

Europe PMC Funders Author Manuscripts

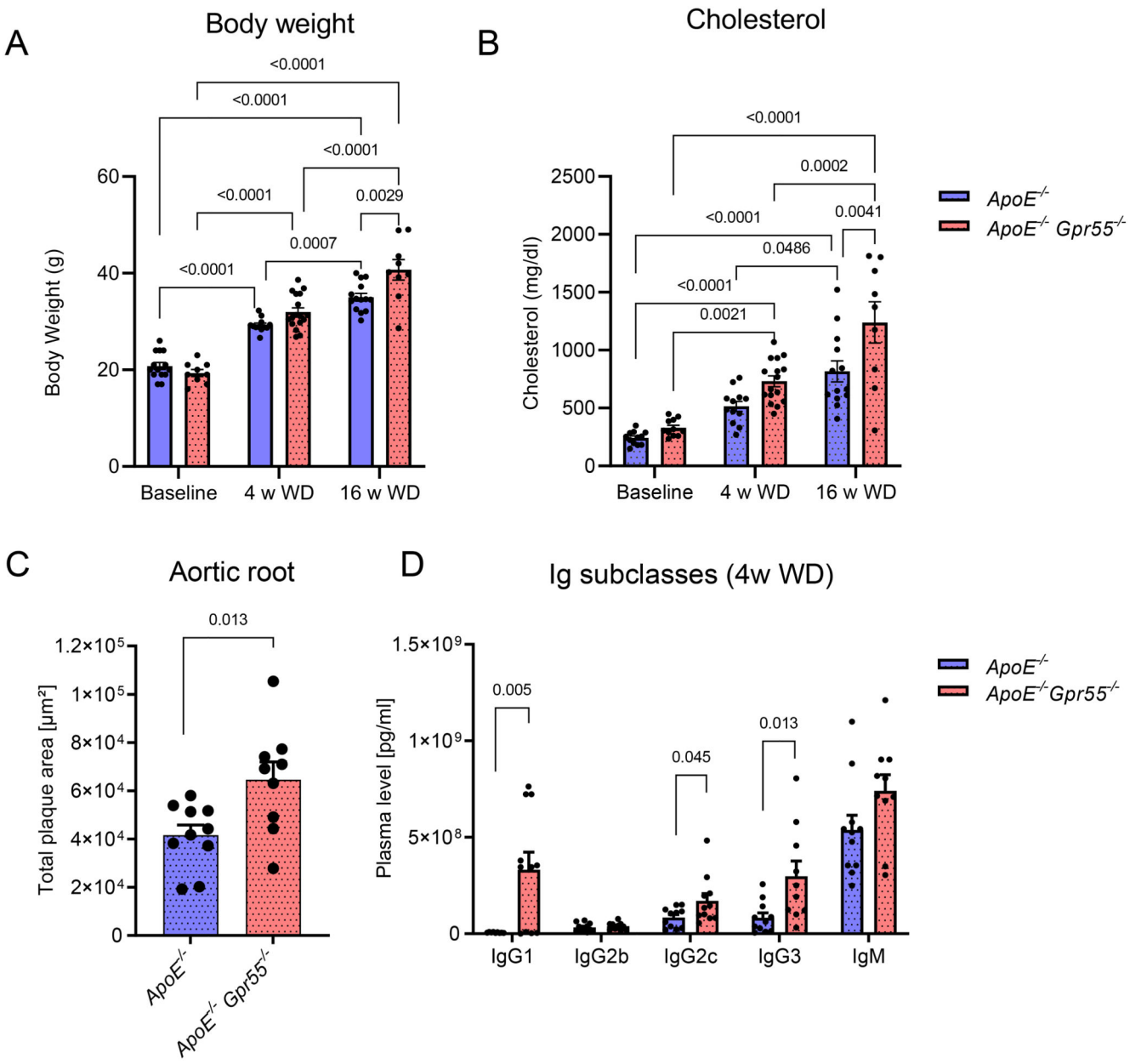

Europe PMC Funders Author Manuscripts

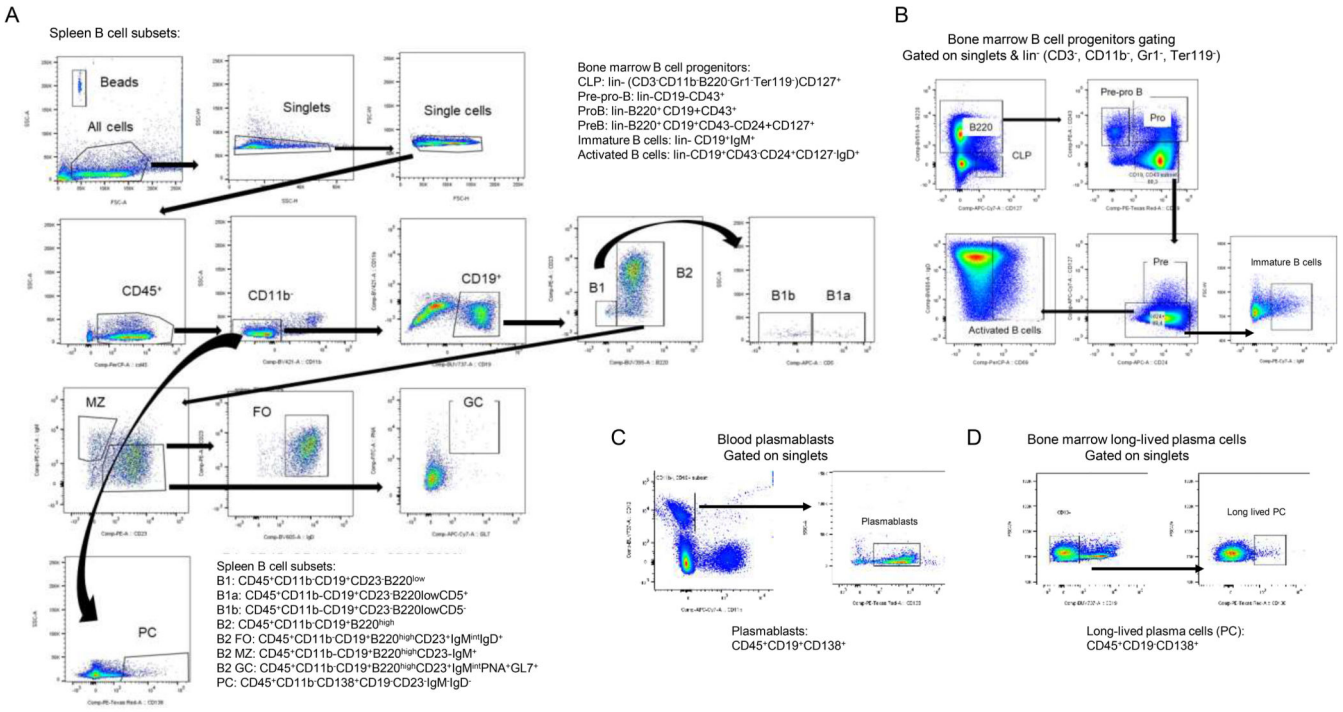

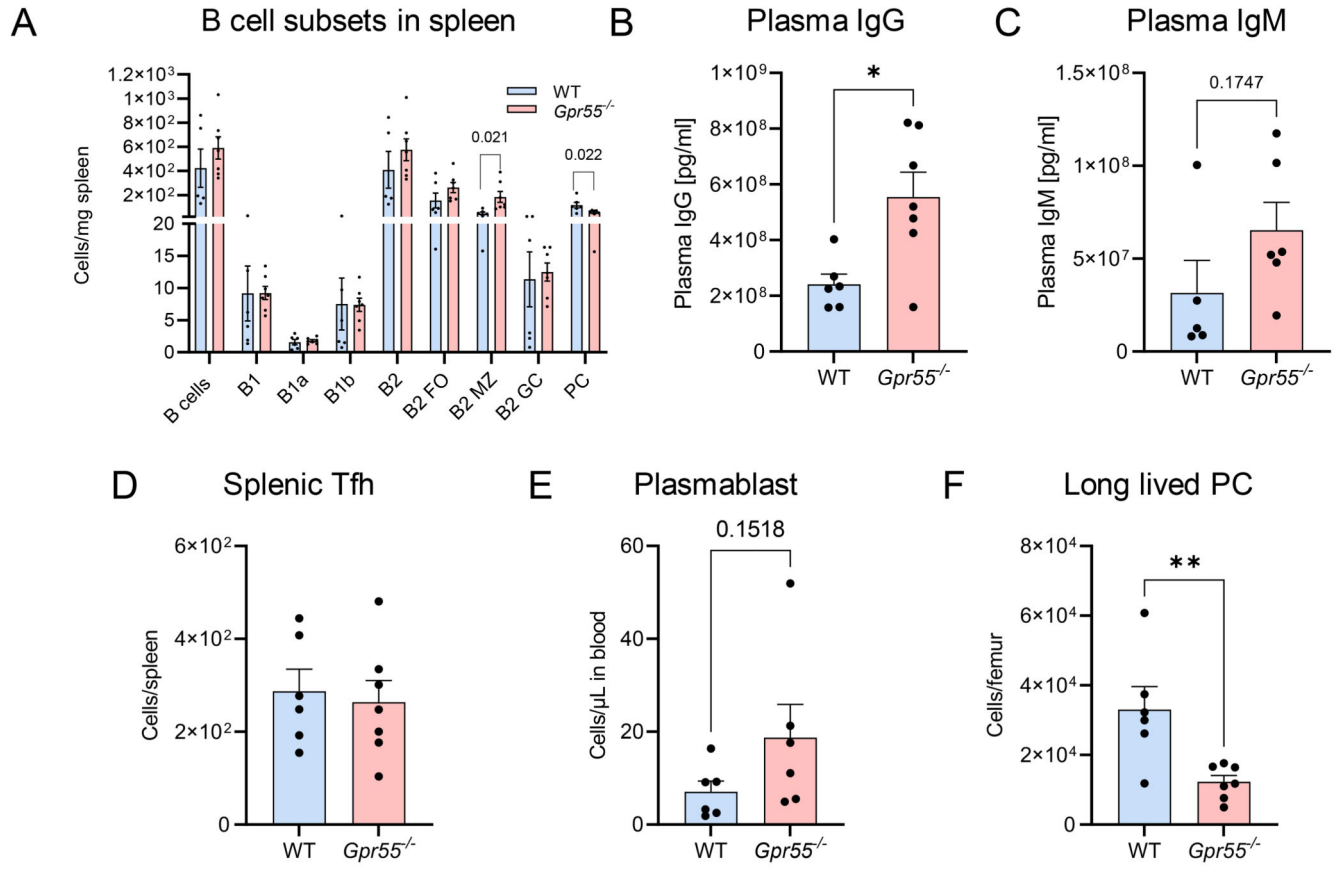

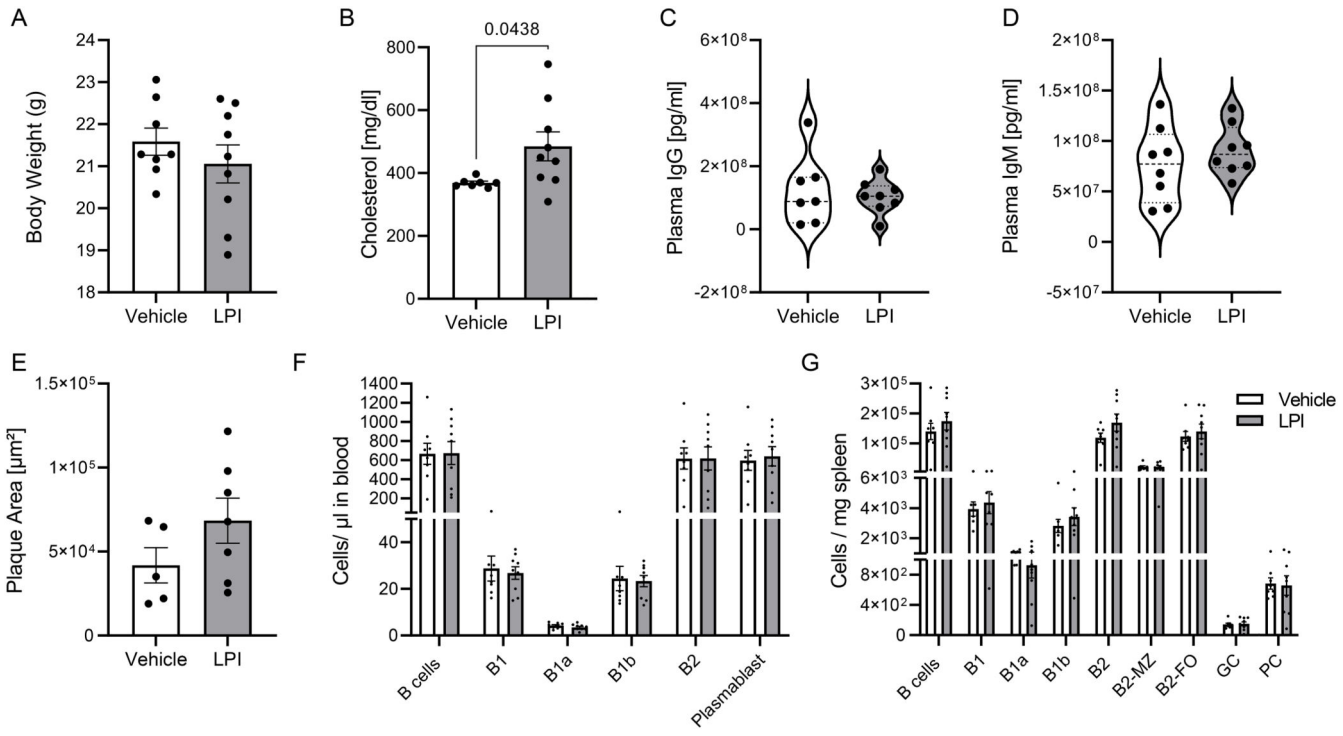

Europe PMC Funders Author Manuscripts

Europe PMC Funders Author Manuscripts

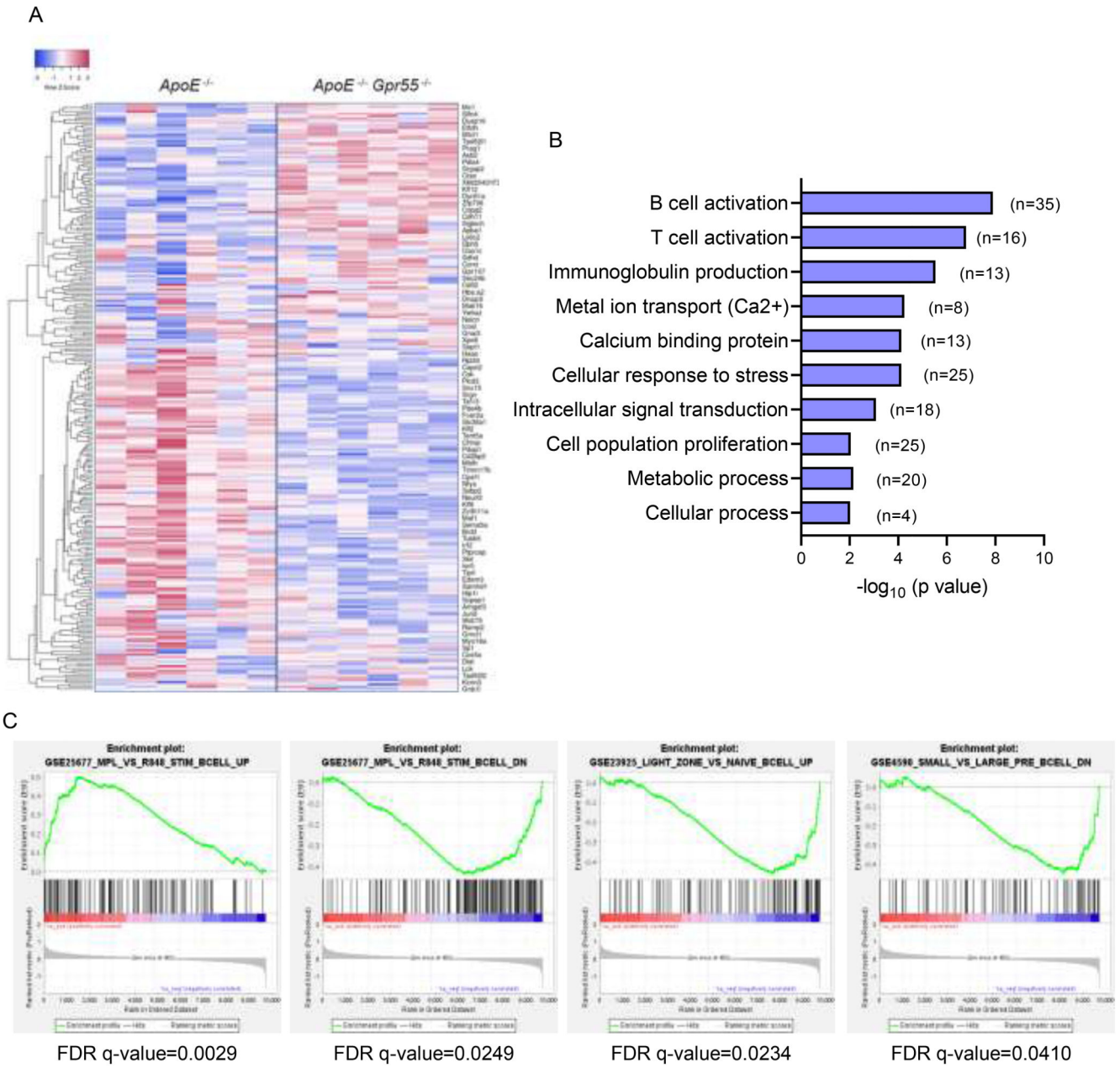

Europe PMC Funders Author Manuscripts

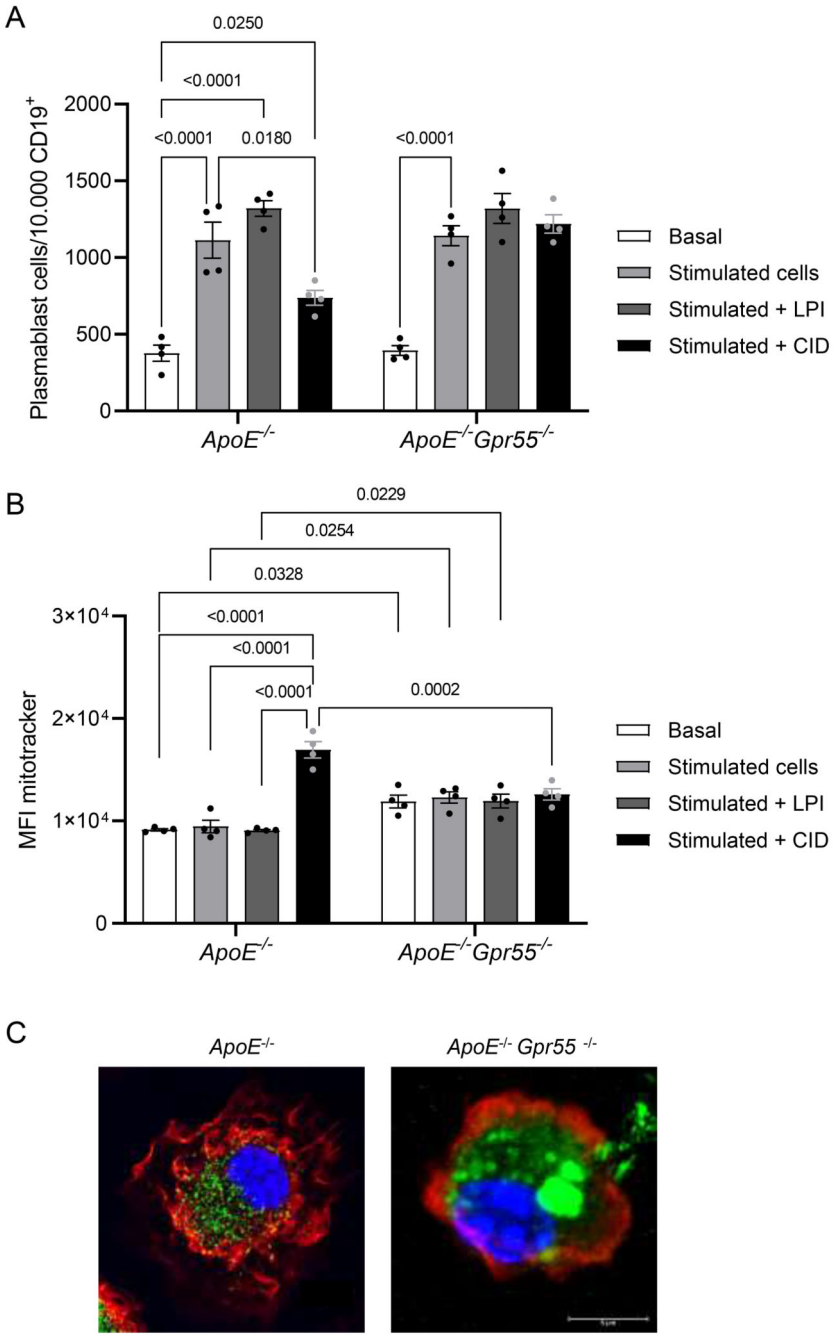

	Stable plaque	Unstable/ruptured plaque
Number of patients	8	8
Age (median)	73	78
BMI (median)	26.2	26.4
Diabetes mellitus (absolute numbers)	2/8	1/8

	Stable plaque	Unstable/ruptured plaque
Sex	2 female / 6 male	3 female / 5 male
Arterial hypertension (absolute numbers)	6/8	6/8
Coronary artery disease (absolute numbers)	4/4	4/4
Hyperlipidemia (absolute numbers)	6/8	7/8
Smoking	5/8	5/8
Symptomatic (stroke, TIA, amaurosis fugax; absolute numbers)	3/8	2/8

Supplementary Material

Refer to Web version on PubMed Central for supplementary material.

Acknowledgements

We are deeply grateful to Maria Aslani for her advice in transcriptomic data visual presentation and thank Diana Wagner, Yvonne Jansen, Rodrigo Carrasco-Leon, Blanca Dufner and Silviya Wolkerstorfer for their excellent technical support.

The authors received funds from the Deutsche Forschungsgemeinschaft (STE1053/6-1, STE1053/8-1 to S.S. and SFB1123 to S.S., C.W. and L.M.), the German Ministry of Research and Education (DZHK FKZ 81Z0600205 to S.S.), the European Research Council (ERC-AdG- 69251 to C.W.), and the LMU Medical Faculty FöFoLe program (1061 to R.G.P.). I.H. is supported by the DFG (HI1573/2 and CRC1425 #422681845).

Data availability

The RNA-sequencing data are accessible under GEO accession number GSE211594.

References

1. Libby P, et al. Atherosclerosis. Nat Rev Dis Primers. 2019; 5: 56. [PubMed: 31420554]
2. Libby P. The changing landscape of atherosclerosis. Nature. 2021; 592: 524–533. [PubMed: 33883728]
3. Galkina E, Ley K. Immune and inflammatory mechanisms of atherosclerosis (*). Annu Rev Immunol. 2009; 27: 165–197. [PubMed: 19302038]
4. Hill CA, Fernandez DM, Giannarelli C. Single cell analyses to understand the immune continuum in atherosclerosis. Atherosclerosis. 2021; S0021-9150(21)00181–7 doi: 10.1016/j.atherosclerosis.2021.04.003
5. Srikakulapu P, McNamara CAB. cells and atherosclerosis. Am J Physiol Heart Circ Physiol. 2017; 312: H1060–H1067. [PubMed: 28314764]
6. Kyaw T, Tipping P, Bobik A, Toh B-H. Opposing roles of B lymphocyte subsets in atherosclerosis. Autoimmunity. 2017; 50: 52–56. [PubMed: 28166680]
7. Aziz M, Holodick NE, Rothstein TL, Wang P. The role of B-1 cells in inflammation. Immunol Res. 2015; 63: 153–166. [PubMed: 26427372]
8. Tsiantoulas D, Diehl CJ, Witztum JL, Binder CJB. cells and humoral immunity in atherosclerosis. Circ Res. 2014; 114: 1743–1756. [PubMed: 24855199]
9. Stebegg M, et al. Regulation of the Germinal Center Response. Front Immunol. 2018; 9 2469 [PubMed: 30410492]
10. Victora GD, Nussenzweig MC. Germinal Centers. Annu Rev Immunol. 2022; 40: 413–442. [PubMed: 35113731]

Europe PMC Funders Author Manuscripts

11. Sage AP, Tsiantoulas D, Binder CJ, Mallat Z. The role of B cells in atherosclerosis. Nat Rev Cardiol. 2019; 16: 180–196. [PubMed: 30410107]
12. Lorenzo C, et al. ALDH4A1 is an atherosclerosis auto-antigen targeted by protective antibodies. Nature. 2021; 589: 287–292. [PubMed: 33268892]
13. Nus M, et al. Marginal zone B cells control the response of follicular helper T cells to a high-cholesterol diet. Nat Med. 2017; 23: 601–610. [PubMed: 28414328]
14. Immunological Genome Project. ImmGen at 15. Nat Immunol. 2020; 21: 700–703. [PubMed: 32577013]
15. Guillamat-Prats R, Rami M, Herzig S, Steffens S. Endocannabinoid Signalling in Atherosclerosis and Related Metabolic Complications. Thromb Haemost. 2019; 119: 567–575. [PubMed: 30769363]
16. Puhl S-L. Cannabinoid-sensitive receptors in cardiac physiology and ischaemia. Biochim Biophys Acta Mol Cell Res. 2020; 1867 118462 [PubMed: 30890410]
17. Drzazga A, Sowińska A, Koziołkiewicz M. Lysophosphatidylcholine and lysophosphatidylinosiol--novel promissing signaling molecules and their possible therapeutic activity. Acta Pol Pharm. 2014; 71: 887–899. [PubMed: 25745761]
18. Sumida H, et al. GPR55 regulates intraepithelial lymphocyte migration dynamics and susceptibility to intestinal damage. Sci Immunol. 2017; 2 eaao1135 [PubMed: 29222090]
19. Lanuti M, Talamonti E, Maccarrone M, Chiurchiù V. Activation of GPR55 Receptors Exacerbates oxLDL-Induced Lipid Accumulation and Inflammatory Responses, while Reducing Cholesterol Efflux from Human Macrophages. PLoS One. 2015; 10 e0126839 [PubMed: 25970609]
20. Wang Y, Pan W, Wang Y, Yin Y. The GPR55 antagonist CID16020046 protects against ox-LDL-induced inflammation in human aortic endothelial cells (HAECs). Arch Biochem Biophys. 2020; 681 108254 [PubMed: 31904362]
21. Montecucco F, et al. Treatment with the GPR55 antagonist CID16020046 increases neutrophil activation in mouse atherogenesis. Thromb Haemost. 2016; 116: 987–997. [PubMed: 27465665]
22. Veillard NR, Steffens S, Burger F, Pelli G, Mach F. Differential expression patterns of proinflammatory and antiinflammatory mediators during atherogenesis in mice. Arterioscler Thromb Vasc Biol. 2004; 24: 2339–2344. [PubMed: 15458979]
23. Stary HC, et al. A definition of advanced types of atherosclerotic lesions and a histological classification of atherosclerosis. A report from the Committee on Vascular Lesions of the Council on Arteriosclerosis American Heart Association. Circulation. 1995; 92: 1355–1374. [PubMed: 7648691]
24. Redgrave JN, Gallagher P, Lovett JK, Rothwell PM. Critical cap thickness and rupture in symptomatic carotid plaques: the oxford plaque study. Stroke. 2008; 39: 1722–1729. [PubMed: 18403733]
25. Horikawa K, et al. Enhancement and suppression of signaling by the conserved tail of IgG memory-type B cell antigen receptors. J Exp Med. 2007; 204: 759–769. [PubMed: 17420266]
26. Haerzschel A, et al. BCR and chemokine responses upon anti-IgM and anti-IgD stimulation in chronic lymphocytic leukaemia. Ann Hematol. 2016; 95: 1979–1988. [PubMed: 27542958]
27. Fondevila MF, et al. The L-α-Lysophosphatidylinositol/G Protein-Coupled Receptor 55 System Induces the Development of Nonalcoholic Steatosis and Steatohepatitis. Hepatology. 2021; 73: 606–624. [PubMed: 32329085]
28. Janjic A, et al. Prime-seq, efficient and powerful bulk RNA-sequencing. bioRxiv. 2021; 2021.09.27.459575 doi: 10.1101/2021.09.27.459575
29. Liu C, et al. CD23 can negatively regulate B-cell receptor signaling. Sci Rep. 2016; 6 25629 [PubMed: 27181049]
30. Kleiman E, et al. Distinct Transcriptomic Features are Associated with Transitional and Mature B-Cell Populations in the Mouse Spleen. Front Immunol. 2015; 6: 30. [PubMed: 25717326]
31. Chevrier S, et al. The BTB-ZF transcription factor Zbtb20 is driven by Irf4 to promote plasma cell differentiation and longevity. J Exp Med. 2014; 211: 827–840. [PubMed: 24711583]
32. Recaldin T, Fear DJ. Transcription factors regulating B cell fate in the germinal centre. Clin Exp Immunol. 2016; 183: 65–75. [PubMed: 26352785]

Europe PMC Funders Author Manuscripts

33. Bhat TA, et al. Endoplasmic reticulum-mediated unfolded protein response and mitochondrial apoptosis in cancer. Biochim Biophys Acta Rev Cancer. 2017; 1867: 58–66. [PubMed: 27988298]
34. Echeverri Tirado LC, Yassin LM. B cells interactions in lipid immune responses: implications in atherosclerotic disease. Lipids Health Dis. 2017; 16: 30. [PubMed: 28166809]
35. Kang S, Lee A-Y, Park S-Y, Liu K-H, Im D-S. O-1602 Promotes Hepatic Steatosis through GPR55 and PI3 Kinase/Akt/SREBP-1c Signaling in Mice. Int J Mol Sci. 2021; 22 3091 [PubMed: 33803038]
36. Console-Bram L, Brailoiu E, Brailoiu GC, Sharir H, Abood ME. Activation of GPR18 by cannabinoid compounds: a tale of biased agonism. Br J Pharmacol. 2014; 171: 3908–3917. [PubMed: 24762058]
37. Stief A, et al. Mice deficient in CD23 reveal its modulatory role in IgE production but no role in T and B cell development. J Immunol. 1994; 152: 3378–3390. [PubMed: 8144922]
38. Payet ME, Woodward EC, Conrad DH. Humoral response suppression observed with CD23 transgenics. J Immunol. 1999; 163: 217–223. [PubMed: 10384119]
39. Yabas M, Yazicioglu YF, Hoyne GF, Goodnow CC, Enders A. Loss of hnRNPLL- dependent splicing of Ptprc has no impact on B-cell development activation and terminal differentiation into antibody-secreting cells. Immunol Cell Biol. 2021; 99: 532–541. [PubMed: 33331104]
40. Xie J-H, Li Y-Y, Jin J. The essential functions of mitochondrial dynamics in immune cells. Cell Mol Immunol. 2020; 17: 712–721. [PubMed: 32523116]
41. Caro-Maldonado A, et al. Metabolic reprogramming is required for antibody production that is suppressed in anergic but exaggerated in chronically BAFF-exposed B cells. J Immunol. 2014; 192: 3626–3636. [PubMed: 24616478]
42. Breda CN, de S, Davanzo GG, Basso PJ, Saraiva Câmara NO, Moraes-Vieira PMM. Mitochondria as central hub of the immune system. Redox Biol. 2019; 26 101255 [PubMed: 31247505]
43. Jang K-J, et al. Mitochondrial function provides instructive signals for activation-induced B- cell fates. Nat Commun. 2015; 6 6750 [PubMed: 25857523]
44. Urbanczyk S, et al. Mitochondrial function is essential for humoral immunity by controlling flux of the TCA cycle, phosphatidic acid and mTOR activity in B cells. 2021; doi: 10.1101/2021.01.14.426649
45. Scharenberg AM, Humphries LA, Rawlings DJ. Calcium signalling and cell-fate choice in B cells. Nat Rev Immunol. 2007; 7: 778–789. [PubMed: 17853903]
46. Rinne P, et al. Palmitoylethanolamide Promotes a Proresolving Macrophage Phenotype and Attenuates Atherosclerotic Plaque Formation. Arterioscler Thromb Vasc Biol. 2018; 38: 2562–2575. [PubMed: 30354245]
47. Puhl S-L, et al. Haematopoietic and cardiac GPR55 synchronize post-myocardial infarction remodelling. Sci Rep. 2021; 11 14385 [PubMed: 34257332]
48. Jin H, et al. Local Delivery of miR-21 Stabilizes Fibrous Caps in Vulnerable Atherosclerotic Lesions. Mol Ther. 2018; 26: 1040–1055. [PubMed: 29503197]
49. Eken SM, et al. MicroRNA-210 Enhances Fibrous Cap Stability in Advanced Atherosclerotic Lesions. Circ Res. 2017; 120: 633–644. [PubMed: 27895035]
50. Bindila L, Lutz B. Extraction and Simultaneous Quantification of Endocannabinoids and Endocannabinoid-Like Lipids in Biological Tissues. Methods Mol Biol. 2016; 1412: 9–18. [PubMed: 27245887]
51. Daugherty A, et al. Recommendation on Design Execution and Reporting of Animal Atherosclerosis Studies: A Scientific Statement From the American Heart Association. Arterioscler Thromb Vasc Biol. 2017; 37: e131–e157. [PubMed: 28729366]
52. Sager HB, et al. RNAi targeting multiple cell adhesion molecules reduces immune cell recruitment and vascular inflammation after myocardial infarction. Sci Transl Med. 2016; 8 342ra80
53. Dobin A, et al. STAR: ultrafast universal RNA-seq aligner. Bioinformatics. 2013; 29: 15–21. [PubMed: 23104886]
54. Subramanian A, et al. Gene set enrichment analysis: a knowledge-based approach for interpreting genome-wide expression profiles. Proc Natl Acad Sci U S A. 2005; 102: 15545–15550. [PubMed: 16199517]

55. Liberzon A, et al. The Molecular Signatures Database (MSigDB) hallmark gene set collection. Cell Syst. 2015; 1: 417–425. [PubMed: 26771021]

56. Liberzon A, et al. Molecular signatures database (MSigDB) 3.0. Bioinformatics. 2011; 27: 1739–1740. [PubMed: 21546393]

57. Godec J, et al. Compendium of Immune Signatures Identifies Conserved and SpeciesSpecific Biology in Response to Inflammation. Immunity. 2016; 44: 194–206. [PubMed: 26795250]

58. Maïga RI, Bonnaure G, Rochette JT, Néron S. Human CD38hiCD138^{+} plasma cells can be generated in vitro from CD40-activated switched-memory B lymphocytes. J Immunol Res. 2014; 2014 635108 [PubMed: 25759831]

59. Jourdan M, et al. An in vitro model of differentiation of memory B cells into plasmablasts and plasma cells including detailed phenotypic and molecular characterization. Blood. 2009; 114: 5173–5181. [PubMed: 19846886]

Europe PMC Funders Author Manuscripts

Europe PMC Funders Author Manuscripts

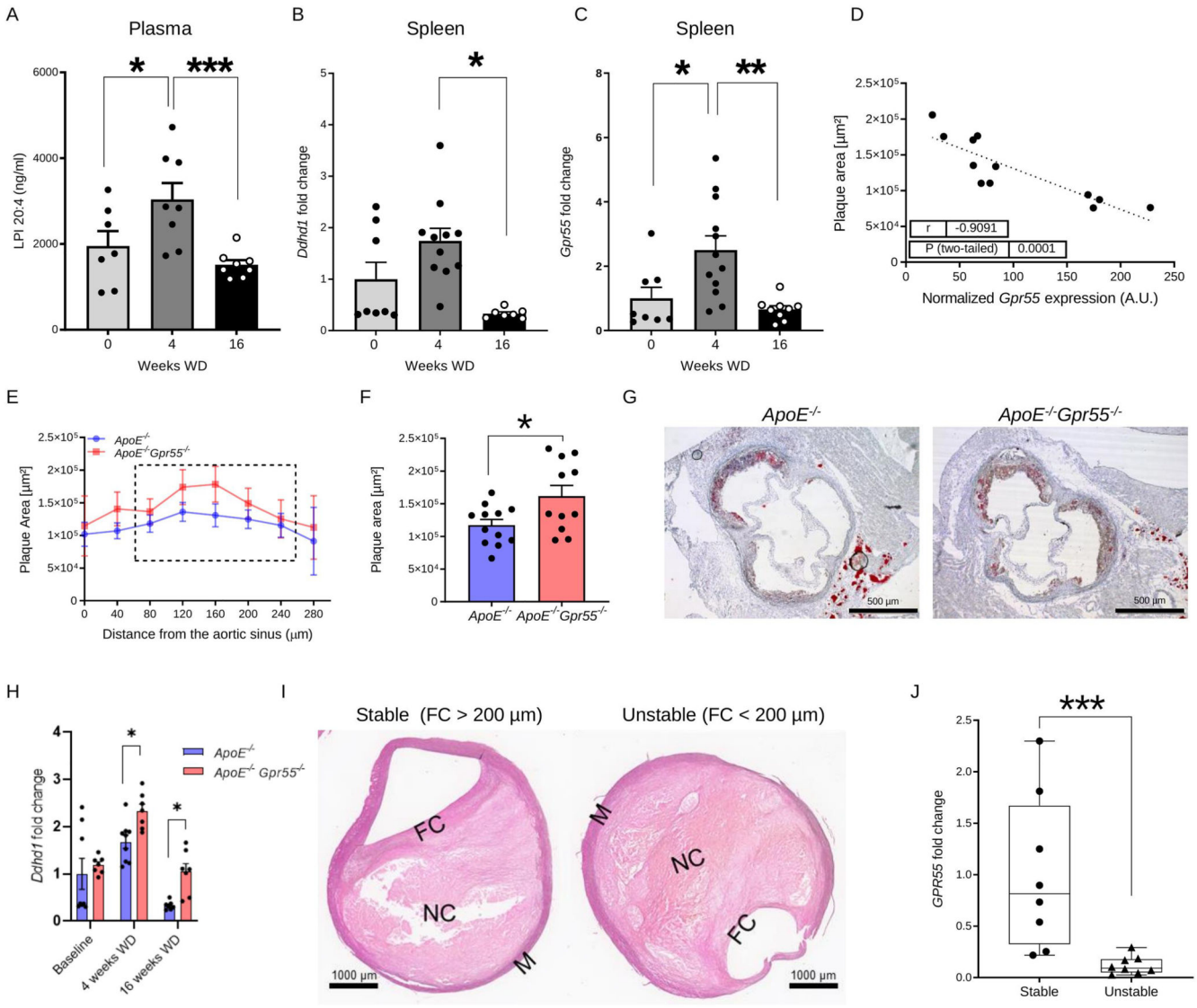

Figure 1. Regulation and function of GPR55 signaling in atherosclerosis.

(**A-D**) Plasma, spleens and aortic roots were collected from *Apoe*$^{-/-}$ mice at baseline or after 4 and 16 weeks WD to determine (**A**) lysophosphatidylinositol (LPI) plasma concentrations (n=7-8; * p=0.05; ***p=0.0042) or (**B-C**) relative splenic mRNA expression of the gene encoding the LPI-synthesizing enzyme DDHD1 (n=7-8; p=0.0018) and the LPI receptor GPR55 (n=7-8; * p=0.019; **p=0.0028). (**D**) Splenic *Gpr55* mRNA expression values were plotted against the aortic root plaque areas of the same mice (n=12). (**E**) Plaque area per aortic root section of female *Apoe*$^{-/-}$ and *Apoe*$^{-/-}$*Gpr55*$^{-/-}$ mice after 4 weeks WD (n=11-12 per group; (* p=0.023). The dotted square indicates the sections used for calculating the average plaque area per animal shown in (**F**). (**G**) Representative Oil-Red-O stains of aortic roots after 4 weeks WD. (**H**) Splenic *Ddhd1* mRNA expression of baseline, 4 and 16 weeks WD *Apoe*$^{-/-}$ and *Apoe*$^{-/-}$*Gpr55*$^{-/-}$ mice, (for baseline n=7-9; for 4 weeks n=6-8 and * p=0.04 and for 16 weeks n=6-7 and *p=0.035) (I) Representative pictures of human stable and unstable plaques (obtained from the Munich Vascular Biobank, shown is one of the eight

samples evaluated. (**J**) Human *GPR55* mRNA expression evaluated by qPCR in stable vs. unstable/ruptured carotid artery plaque corrected by *RPLPO* used as housekeeping control (*** p=0.0006). The box plot shows the min to max value and each dot represents one patient. Mouse data shown in A-F were combined from 3 independent experiments, each dot represent one biologically independent mouse sample. All data are shown as mean ± SEM. Two-sided unpaired Student's t-test or one-Way-ANOVA followed by a post-hoc Newman–Keuls multiple-comparison test was used to determine the significant differences. Bivariate correlation was analyzed by Spearman's rank correlation test. FC, fibrous cap; LPI, lysophosphatidylinositol; M, media; NC, necrotic core; WD, Western diet.

Europe PMC Funders Author Manuscripts

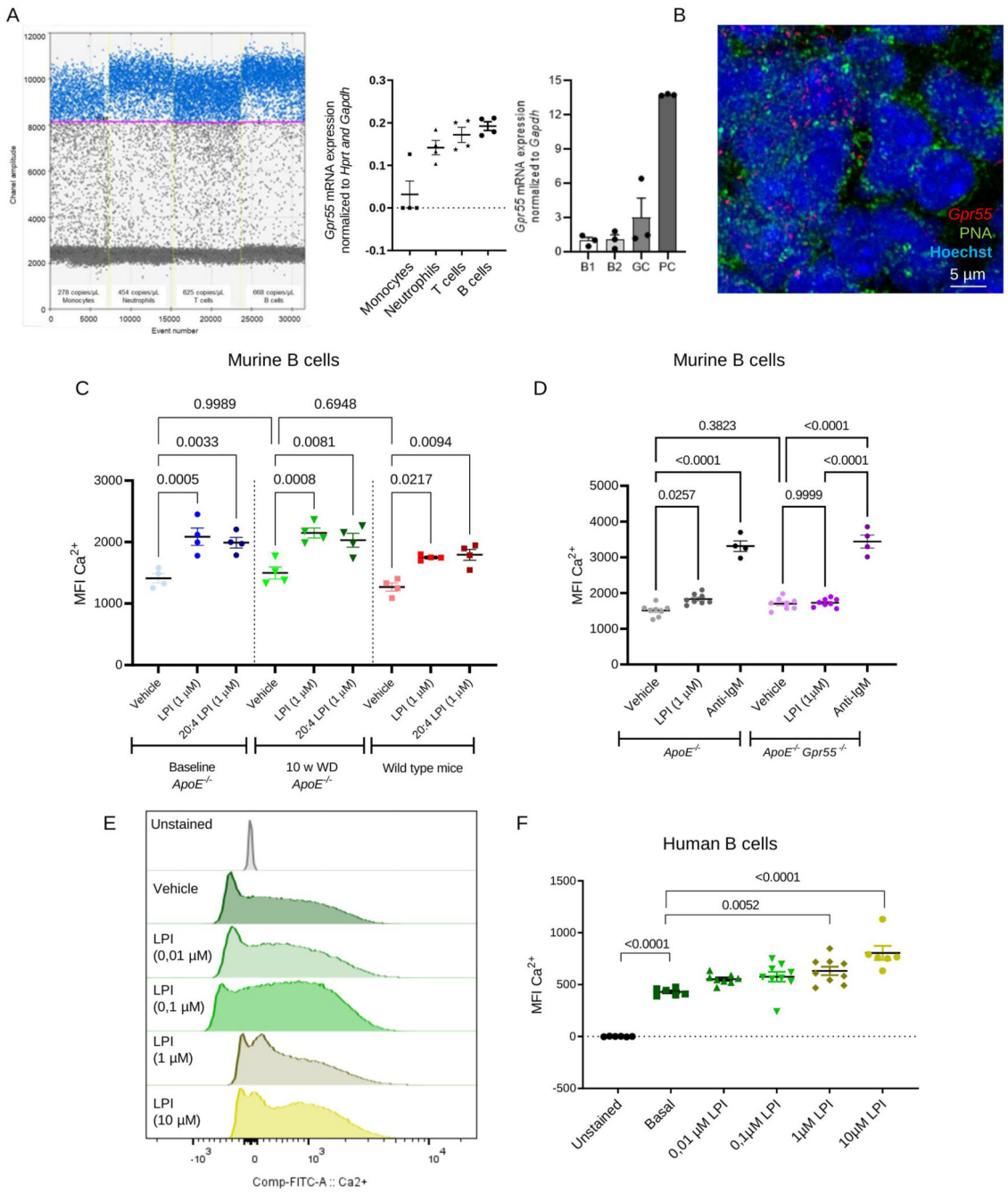

Figure 2. GPR55 expression and Ca^{2+} responses in murine and human B cells.

(**A**) *Gpr55* mRNA expression determined by digital droplet PCR (left) and qPCR (right) in sorted circulating leukocyte subsets and splenic B cell subsets. Each dot represents sorted cells isolated from a biologically independent *Apoe*$^{-/-}$ mouse sample (n=3-4). (**B**) *In situ* hybridization to detect *Gpr55* (red) in splenic GC areas (PNA^{+}, green; nuclei, blue). The assay was performed with 3 independent *Apoe*$^{-/-}$ mouse samples. (**C**) Average mean fluorescence intensity (MFI) of intracellular Ca^{2+} sensor in circulating B cells of *Apoe*$^{-/-}$ mice under normal diet (baseline) or 10 weeks Western Diet and C57BL/6J wild type mice

Europe PMC Funders Author Manuscripts

Europe PMC Funders Author Manuscripts

under normal diet, in response to soybean LPI or pure 20:4 LPI stimulation (n=4). (**D**) Average mean fluorescence intensity (MFI) of intracellular Ca^{2+} sensor in circulating B cells of *Apoe*$^{-/-}$ and *Apoe*-/-*Gpr55*-/-. mice in response to LPI or anti-IgM stimulation (n=4-8). (**E**) Representative histogram and (**F**) average MFI of intracellular Ca^{2+} sensor in human B cells at baseline conditions and after addition of vehicle or LPI. Data were combined from 2 independent experiments, and each dot represent one biologically independent mouse or human sample (n=7-8) All data are shown as mean ± SEM). One-Way-ANOVA followed by a post-hoc Newman–Keuls multiple-comparison or two-way-ANOVA followed with Kruskal–Wallis test with Dunn post hoc test was used to evaluate the significant differences. GC, germinal center; LPI, lysophosphatidylinositol; MFI, mean fluorescence intensity; PC, plasma cell; w, weeks; WD, Western diet.

Europe PMC Funders Author Manuscripts

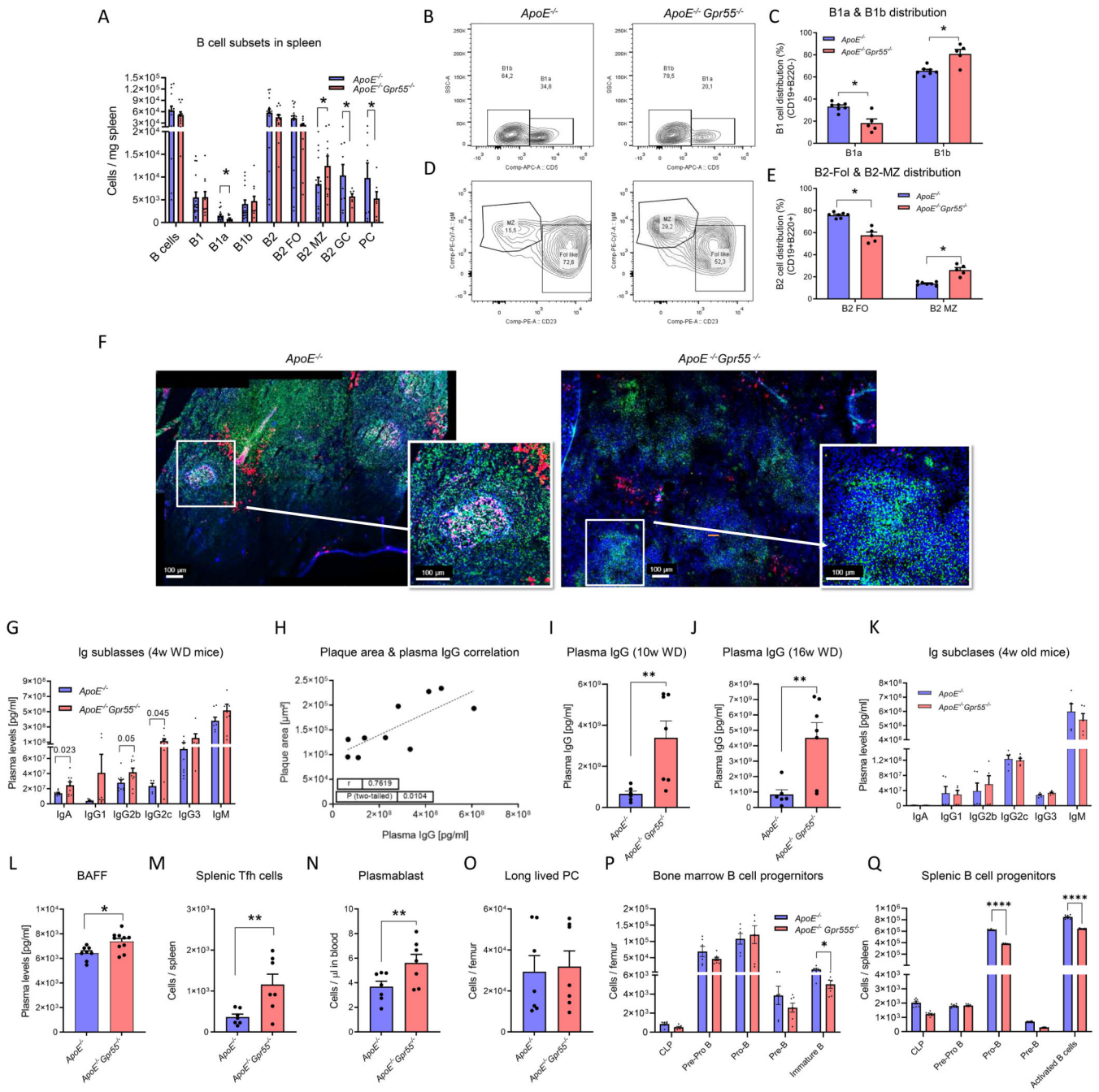

Figure 3. B cell immunoprofiling of global *Gpr55*-deficient mice after 4 weeks WD.

(**A**) Splenic B cell subsets quantified by flow cytometry (n=15-16; * p=0.05). (**B, C**) Representative gating strategy and relative proportion of B1 cell subsets. (**D, E**) Representative gating strategy and relative proportion of B2 cell subsets (n=5-7; * p=0.05). (**F**) Confocal imaging of spleen sections stained for B cell markers PNA (GC, green), IgM (MZ or memory B cells, red), CD23 (FO B cells, pink) and nuclei (blue). Six independent samples were analysed. (**G**) Plasma Ig titers (n=6-9) and (**H**) IgG titers plotted against aortic plaque size in *Gpr55*-deficient mice (n=10) (**I**) Plasma IgG titers in mice after 10 (n=6-7;

*p=0.0047) **(J)** or 16 weeks Western diet (n=6-7; *p=0.0045). (**K**) Plasma Ig titers in young 4-week-old mice (n=5) (**L**). B cell activating factor (BAFF) concentrations after 4 weeks WD (n=8-10; **p=0.0098). (**M**) Number of splenic T follicular helper (Tfh) cells (n=7; **p=0.010)., (**N**) circulating plasmablasts (n=7; **p=0.035). and (**O**) long-lived plasma cells (PC) in bone marrow assessed by flow cytometry after 4 weeks WD. (**P**) Lymphoid B cell progenitors in the bone marrow (n=5-7; *p=0.05). and (**Q**) spleen after 4 weeks WD (n=5-7; **** p<0.0001). Data were combined from 2 independent experiments for all figure panels, and each dot represent one biologically independent mouse sample (mean ± SEM). Two-sided unpaired Student's t-test was used to determine the significant differences. BAFF, B-cell activating factor; GC, germinal center; FO, follicular; Ig, immunoglobulins; MZ, marginal zone; PC, plasma cell; w, weeks; WD, Western diet.

Europe PMC Funders Author Manuscripts

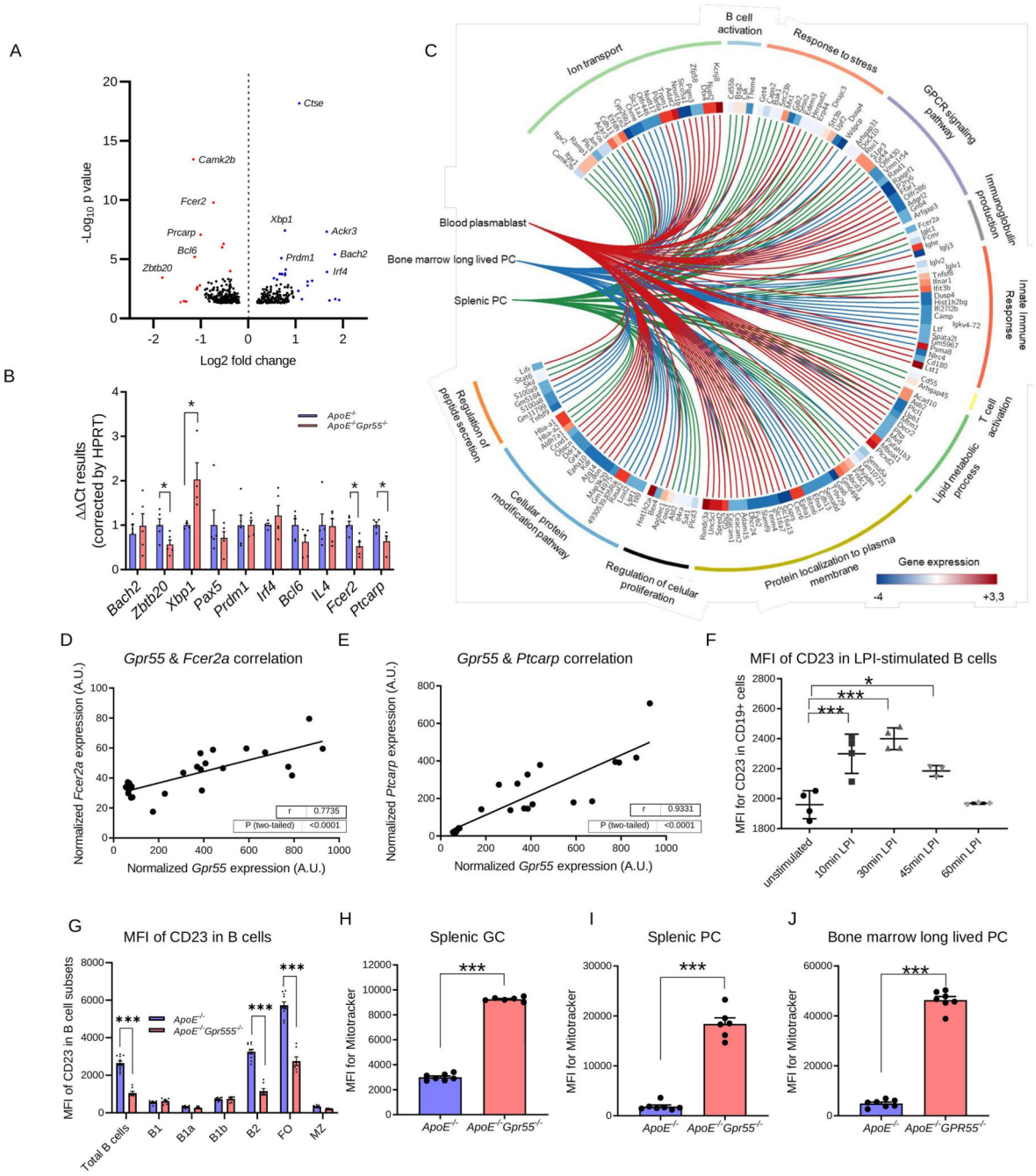

Figure 4. Impact of global *GPR55* deficiency on B cell transcriptome and mitochondrial content

(**A**) Volcano plot of differentially expressed genes (DEGs) in *Apoe*$^{-/-}$*Gpr55*$^{-/-}$ versus *Apoe*$^{-/-}$ splenic CD19+ cells after 4 weeks WD. The x-axis shows log2 fold changes between genotypes. The y-axis plots negative log10 P-values computed by DEseq2 (based on a generalized linear model) and corrected for multiple comparisons according to the Benjamini-Hochberg FDR; relevant statistically upregulated (blue) and downregulated (red) genes are highlighted; n=6). (**B**) Confirmation of the main DEGs in splenic B cells of *Apoe*$^{-/-}$*Gpr55*$^{-/-}$ compared to *Apoe*$^{-/-}$ mice after 4 weeks WD by qPCR (n=5; p=0.05). (**C**)

Chord diagram showing the main regulated genes and pathways in splenic *Apoe*$^{-/-}$*Gpr55*$^{-/-}$ versus *Apoe*$^{-/-}$ B cells, splenic PCs and circulatory plasmablasts, based on RNA-sequencing. (**D**) Splenic B cell *Gpr55* mRNA expression (qPCR) correlated with *Fcer2a* (CD23 encoding gene) mRNA expression and (**E**) splenic B cell *Gpr55* mRNA expression (qPCR) correlated with *Ptcarpc* (LPAP encoding gene) mRNA expression (n=20 *Apoe*$^{-/-}$ mice). (**F**) Mean fluorescence intensity (MFI) of CD23 on splenic *Apoe*$^{-/-}$ B cells measured by flow cytometry after LPI treatment (1 μM; n=4). (**G**) Flow cytometric analysis of CD23 MFI on splenic B cell subsets of *Apoe*$^{-/-}$ and *Apoe*$^{-/-}$*Gpr55*$^{-/-}$ mice after 4 weeks WD (n=8-10; ***p<0.0001). (**H**) Mitochondrial content of splenic GC B cells (n=6-7; ***p < 0.0001). (**I**) Mitochondrial content of splenic PCs (n=6-7; ***p < 0.0001). (**J**) Mitochondrial content of bone marrow long-lived PCs (n=6-7; ***p < 0.001). Data shown in D-J were combined from 2 independent experiments, and each dot represent one biologically independent mouse sample for all figure panels (mean ± SEM). Two-sided unpaired Student's t-test or one-way-ANOVA followed by a post-hoc Newman–Keuls multiple-comparison test was used to determine the significant differences. Bivariate correlations were analyzed by Spearman's rank correlation test. FO, follicular; GC, germinal center; LPI, lysophosphatidylinositol; MFI, mean fluorescence intensity; MZ, marginal zone; PC, plasma cell.

Europe PMC Funders Author Manuscripts

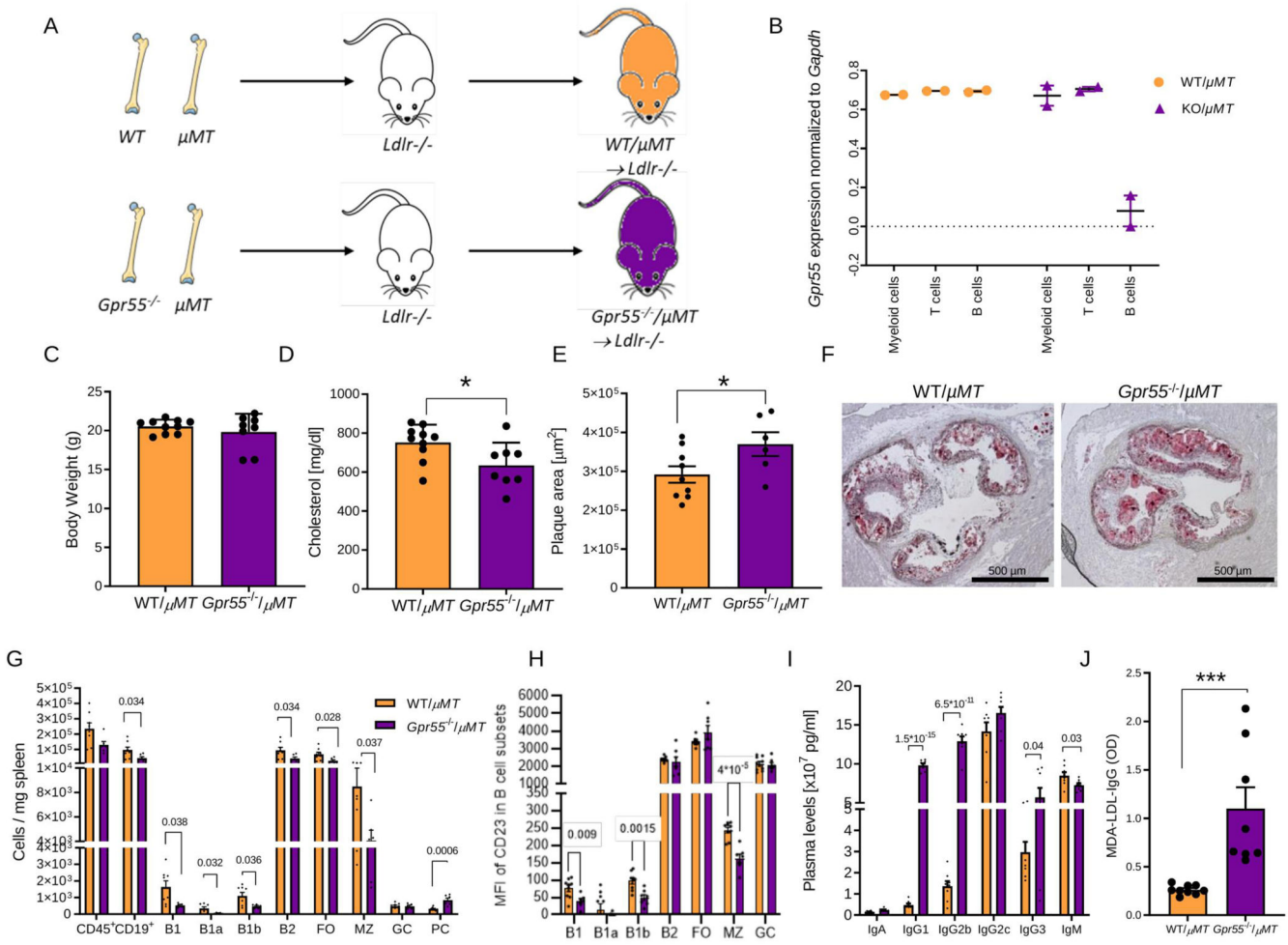

Figure 5. Impact of B cell-specific *Gpr55* deficiency on atherosclerotic plaque development and B cell responses during hypercholesterolemia.

(**A**) Experimental design of the bone marrow transplantation to generate mixed bone marrow chimeras with B cell-specific *Gpr55* deficiency. Lethally irradiated *Ldlr*$^{-/-}$ mice received a 50/50 mixture of *μMT* marrow and *Gpr55*$^{-/-}$ or WT marrow cells. (**B**) Following 6 weeks recovery after the bone marrow transplantation, *Gpr55* expression was measured by qPCR in sorted blood myeloid cells (Cd11b^{+}), T cells (CD3^{+}) and B cells (B220^{+}) to determine the B cell *Gpr55* depletion efficiency in *Gpr55*$^{-/-}$*/μMT* → *Ldlr*$^{-/-}$ mice (n=2). (**C**) Body weight (n=8-9) and (**D**) total plasma cholesterol concentration after 10 weeks WD (n=8-9; * p=0.029). (**E**) Plaque area in aortic roots of bone marrow chimeric female mice after 10 weeks WD (n=6-8; p=0.049). (**F**) Representative Oil-Red-O stained aortic root sections used for plaque quantification. (**G**) Splenic B cell subsets assessed by flow cytometry (n=6-8; exact p value is shown for each Ig subset in the graph). (**H**) Average mean fluorescence intensity (MFI) of CD23 in the different B cell subsets (n=7-9; exact p value is shown for each B cell subset in the graph). **(I)** Plasma Ig titers at the end of the experiment (n=6-8; exact p value is shown for each Ig subset in the graph). (**J**) IgG antibodies against MDA-oxLDLin plasma after 10 weeks WD (n=8-9; ***p=0.0011). Data were obtained in one bone marrow transplantation experiment; and each dot represent one

biologically independent mouse sample (mean ± SEM). Two-sided unpaired Student's t-test was used to determine the significant differences. FO, follicular; GC, germinal center; LPI, lysophosphatidylinositol; MFI, mean fluorescence intensity; MZ, marginal zone; PC, plasma cell; WT, wildtype.

Europe PMC Funders Author Manuscripts

Europe PMC Funders Author Manuscripts

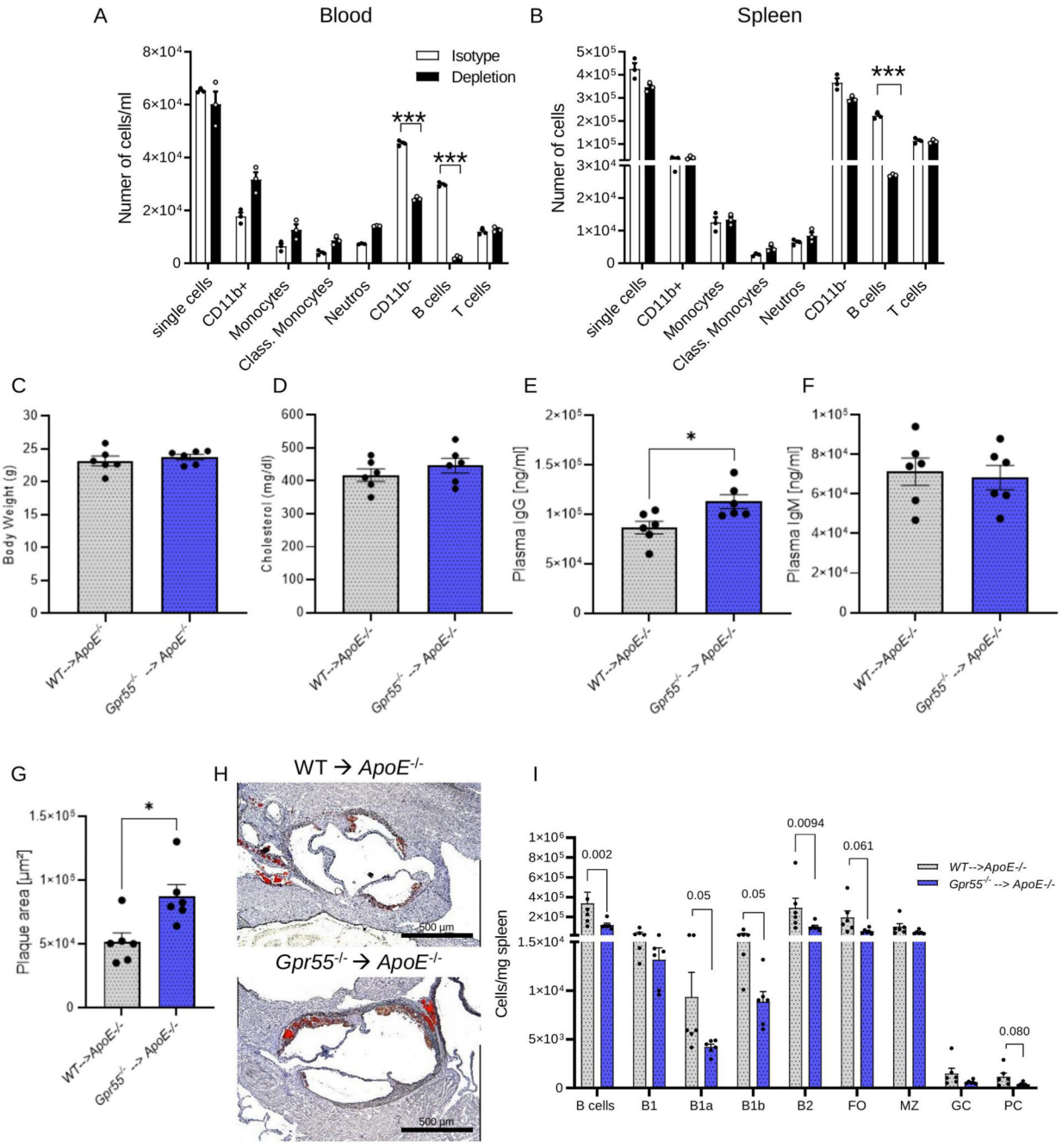

Figure 6. Impact of WT and *Gpr55*$^{-/-}$ adoptive B cell transfer into global *Apoe*$^{-/-}$ mice on atherosclerotic plaque formation and Ig titers

(A) Circulating and (B) splenic leukocyte counts in *Apoe*$^{-/-}$*Gpr55*$^{-/-}$ mice treated with the B cell depletion cocktail or control animals treated with the respective isotype antibodies (n=3 per group; ***p<0.0001). (C) Average body weight (n=6), (D) total plasma cholesterol (n=6), (E) IgG (n=6; p=0.0125) (F) and IgM titers after 4 weeks Western diet (WD). (G) Aortic root plaque size (n=6; p=0.021), and (H) representative oil red O-stained sections of B cell-depleted female *Apoe*$^{-/-}$ mice receiving WT or *Gpr55*$^{-/-}$ B cell adoptive transfer and subsequent WD feeding for 4 weeks; here we show one representative picture of the six per

group that were evaluated. (I) Splenic B cell subsets quantified by flow cytometry (n=6). Data were obtained in one experiment (mean ± SEM; n=6 per group). Two-sided unpaired Student’s t-test was used to determine the significant differences..

Europe PMC Funders Author Manuscripts